



Advanced Study of Switchable Spin Crossover Compounds

Gavin Craig

ADVERTIMENT. La consulta d'aquesta tesi queda condicionada a l'acceptació de les següents condicions d'ús: La difusió d'aquesta tesi per mitjà del servei TDX (www.tdx.cat) i a través del Dipòsit Digital de la UB (diposit.ub.edu) ha estat autoritzada pels titulars dels drets de propietat intel·lectual únicament per a usos privats emmarcats en activitats d'investigació i docència. No s'autoritza la seva reproducció amb finalitats de lucre ni la seva difusió i posada a disposició des d'un lloc aliè al servei TDX ni al Dipòsit Digital de la UB. No s'autoritza la presentació del seu contingut en una finestra o marc aliè a TDX o al Dipòsit Digital de la UB (framing). Aquesta reserva de drets afecta tant al resum de presentació de la tesi com als seus continguts. En la utilització o cita de parts de la tesi és obligat indicar el nom de la persona autora.

ADVERTENCIA. La consulta de esta tesis queda condicionada a la aceptación de las siguientes condiciones de uso: La difusión de esta tesis por medio del servicio TDR (www.tdx.cat) y a través del Repositorio Digital de la UB (diposit.ub.edu) ha sido autorizada por los titulares de los derechos de propiedad intelectual únicamente para usos privados enmarcados en actividades de investigación y docencia. No se autoriza su reproducción con finalidades de lucro ni su difusión y puesta a disposición desde un sitio ajeno al servicio TDR o al Repositorio Digital de la UB. No se autoriza la presentación de su contenido en una ventana o marco ajeno a TDR o al Repositorio Digital de la UB (framing). Esta reserva de derechos afecta tanto al resumen de presentación de la tesis como a sus contenidos. En la utilización o cita de partes de la tesis es obligado indicar el nombre de la persona autora.

WARNING. On having consulted this thesis you're accepting the following use conditions: Spreading this thesis by the TDX (www.tdx.cat) service and by the UB Digital Repository (diposit.ub.edu) has been authorized by the titular of the intellectual property rights only for private uses placed in investigation and teaching activities. Reproduction with lucrative aims is not authorized nor its spreading and availability from a site foreign to the TDX service or to the UB Digital Repository. Introducing its content in a window or frame foreign to the TDX service or to the UB Digital Repository is not authorized (framing). Those rights affect to the presentation summary of the thesis as well as to its contents. In the using or citation of parts of the thesis it's obliged to indicate the name of the author.

ADVANCED STUDY OF SWITCHABLE SPIN CROSSOVER COMPOUNDS

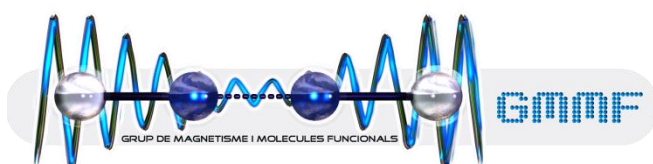
Universitat de Barcelona

Facultat de Química

Departament de Química Inorgànica

Programa de Doctorat: Química Inorgànica Molecular

Grup de Magnetisme i Molècules Funcionals



Gavin Craig

Director: Dr. Guillem Aromí Bedmar, Departament de Química Inorgànica

Tutor: Dr. Santiago Alvarez Reverter, Departament de Química Inorgànica

Contents

Chapter 1: Introduction	1
1.0 Introduction to Spin Crossover (SCO)	1
1.1 Methods of measurement	4
1.1.1 SQUID Magnetometry	4
1.1.2 Single crystal X-ray diffraction	5
1.1.3 Differential Scanning Calorimetry (DSC)	6
1.1.4 Raman spectroscopy	6
1.2 Thermodynamic considerations	7
1.3 Trapping of meta-stable high spin states	8
1.4 Latest advances and applications	11
1.4.1 Beyond bi-stability	12
1.4.2 Physical control of domains	13
1.4.3 Size reduction	15
1.4.4 Detection of SCO on increasingly small scales	17
1.4.5 SCO materials as fluorescent thermometers	18
1.5 2,6-Bis(pyrazol-3-yl)pyridine	20
1.6 Aim and scope of the thesis	28
1.7 References	30

Chapter 1: Introduction

The study of molecular magnetic materials prompted Robertson and Lees to compare the role of the synthetic inorganic chemist to that of a medicinal chemist searching for a new drug.¹ By starting from promising building blocks, the magnetic properties of systems can be studied in a systematic fashion, with this approach aided immeasurably by structural data. One of the fundamental components of this research is the ligand employed to chelate a metal centre, for two significant reasons: i) its shape can help to guide the topology of a novel material, and ii) its donor atoms are the first contribution towards forming the material's electronic properties. An important class of materials within this field is composed of Spin Crossover (SCO) compounds. The study of these systems has entailed unveiling the underlying reasons for its occurrence in terms of coordination chemistry and thermodynamics, the discovery of new methods both to induce the phenomenon and to measure it, and the development of novel compounds.

1.0 Introduction to Spin Crossover (SCO)

Due to the way in which the $3d$ orbitals of first row transition metals split in a pseudo-octahedral ligand field, the electrons of the d^4 - d^7 ions may be distributed in two different configurations.² One corresponds to the maximum possible spin pairing, and is referred to as the low spin (LS) state. The other presents the maximum multiplicity for the given ion, and is therefore denoted the high spin (HS) state. Which of these two possible states is observed for a given system under a set of conditions is dependent on the strength of the ligand field, Δ , created by the ligating species surrounding the metal ion in its first coordination sphere (See Figure 1.1 for the case of d^6 ions). When Δ is strong and results in a greater splitting of the two sets of orbitals, the favoured configuration is the LS state, with this situation reversed when a weaker Δ causes a splitting of lower energy than that required to pair the electrons within the orbitals. Occasionally, the balance between these two states is so delicate that the modulation of an external parameter is sufficient to reversibly switch between them in a phenomenon known as Spin Crossover (SCO).³ While it has been observed in Mn(III),⁴⁻⁶ Fe(III),⁷⁻¹² and Co(II),¹³⁻¹⁵ the vast majority of SCO systems contain Fe(II),¹⁶ which will be the focus of this thesis and, more immediately, the following discussion.

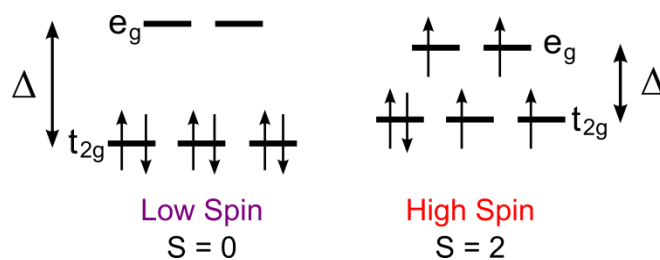


Figure 1.1: The two possible spin states for a d^6 metal ion when the orbitals are split by an octahedral ligand field, Δ .

SCO may be observed in an Fe(II) system when the splitting Δ induced by a given ligand set lies close to the discontinuity observed in the corresponding Tanabe Sugano diagram for the metal ion. Therefore, the possible spin transition is between a 1A_1 singlet state and a 5T_2 quintet state. The splitting Δ is sensitive to both the nature of the ligand and the metal-donor atom distance. This leads to two relative displacements of the potential energy wells for the high and low spin configurations along the symmetric stretch vibration, represented in Figure 1.2.¹⁷ The horizontal displacement of the wells, Δr_{HL} , is due to the population of the anti-bonding e_g orbitals in the quintet state, which causes longer metal-donor atom bond lengths than for the singlet state (typically, $\Delta r_{\text{HL}} \sim 0.2 \text{ \AA}$). The vertical displacement is the difference in the zero-point energies of the two configurations, such that if it is of the order of $k_B T$ thermal SCO may be observed. At low temperatures, there will be a majority population of the LS state, with the HS being increasingly formed at higher temperatures. Temperature variation is in fact the most common method to switch between the spin states, although it can also be achieved through irradiation with light,¹⁸⁻²¹ the application of pressure,²²⁻²⁴ the application of an external magnetic field,²⁵ or the insertion of a guest molecule into the system.²⁶⁻²⁹

A spin transition may be represented as the fraction of Fe(II) ions that are in the HS state, γ_{HS} , vs. a dependent variable, such as the temperature. The difference in physical properties between the two spin states allows for a variety of measurement techniques to be able to derive the populations of each (see Section 1.1). The shapes of these spin transition curves lead to classifications of the SCO behaviour observed, where the temperature at which half of the Fe(II) centres are in either state is denoted $T_{1/2}$ (Figure 1.3 displays some of the more common types).³⁰ The first, a gradual transition, refers to the case where the switch to the LS state takes place over a wide temperature range (tens

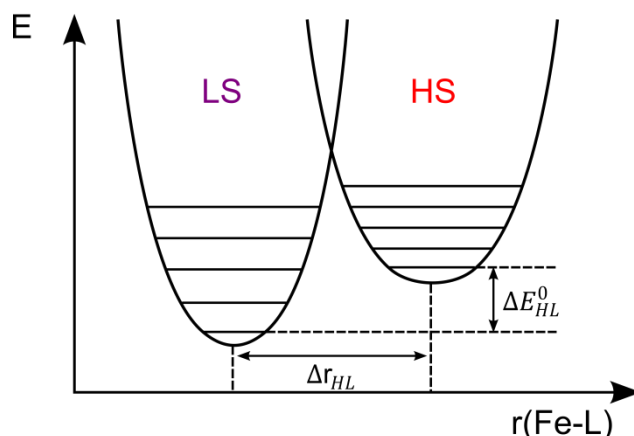


Figure 1.2: The relative displacements of the potential wells corresponding to the two possible spin states as a function of Fe-donor atom distance, along the symmetric metal-ligand stretching vibration.

of Kelvin). This type of transition is often observed in solution,³¹⁻³⁴ where essentially a Boltzmann population of the quintet state is registered with increasing temperature. In the second, an abrupt transition, the SCO process occurs in a much narrower range of temperature, usually less than 10 K. The third illustrated curve presents hysteresis. In this case, there are two values of $T_{1/2}$, one at a lower temperature for the cooling mode than for the heating mode, leading to a bi-stable region in which the state of the system depends on its thermal history. In terms of potential applications, this last scenario is the most desirable because the co-existence of two spin states at the same temperature is directly analogous to having an “on” and an “off” within the system.³⁵ Although not illustrated in the Figure, incomplete transitions where the system doesn’t fully occupy one

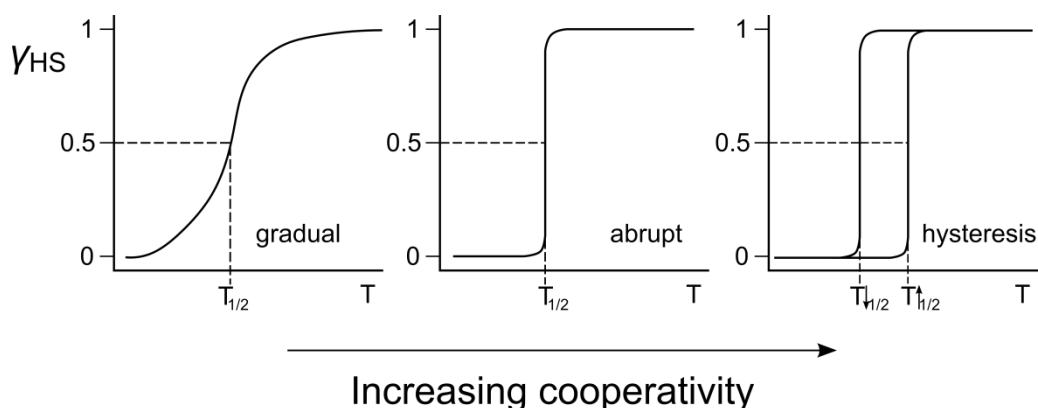


Figure 1.3: Plots illustrating three different types of spin transition curve, as followed by the variation with temperature of the normalised HS fraction, γ_{HS} . Adapted from reference 16.

of the spin states, and stepped transitions where the system passes through an intermediate phase between the high and low spin states, have also been observed.

The decisive factor behind the transitions shown in Figure 1.3 is the concept of cooperativity. The origin of cooperativity lies in the volume change that occurs around the metal ion when it changes spin state, which induces elastic interactions throughout the system, normally mediated by intermolecular contacts.³⁶⁻³⁸ The higher the cooperativity in a SCO system, the more abrupt the transition will be and a spin transition with hysteresis occurs when it is particularly high. Therefore, three strategies have been outlined to increase cooperativity³⁹ within SCO compounds: i) link the SCO centres through bonds, as in polymers; ii) induce greater degrees of hydrogen bonding via the design of appropriate ligands; and iii) favour the formation of $\pi \cdots \pi$ interactions brought about by the shape of the ligands or spin-active entities. These considerations guide the design of the chelating molecules used to synthesise potential SCO systems (Section 1.5).

1.1 Methods of measurement

The marked difference in physical properties between the two different spin states means that a variety of experimental techniques can be used to detect and follow the progress of a spin transition. The following will provide a brief description of how the following techniques have been employed in this thesis, and is therefore not a comprehensive list of the available methods for tracking a spin crossover process.

1.1.1 SQUID Magnetometry

When a material is exposed to a homogeneous external magnetic field, H , a magnetisation M is induced in the sample. If the applied field is not too strong, the degree of magnetisation in the sample may be expressed as the magnetic susceptibility χ_v , defined by Equation 1.1:⁴⁰

$$\chi_v = \frac{M}{H} \quad (1.1)$$

$$\chi_g = \frac{\chi_v}{\rho} \quad (1.2)$$

$$\chi_m = \chi_g \times \frac{M_r}{m} + \left(\frac{M_r}{2} \times 10^{-6} \right) \quad (1.3)$$

This measured susceptibility contains two components, one paramagnetic, which originates from a permanent magnetic dipole moment that acts in the direction of the

applied field, and one diamagnetic, which is a distortion that causes a very small magnetic moment that acts against the applied field. The paramagnetic contribution is positive and much larger than the negative diamagnetic contribution. The molar magnetic susceptibility χ_m can then be obtained through Equation 1.3, where M_r is the molar mass of the compound, m is the mass of the sample, and $M_r/2$ is the approximation used (rather than Pascal's constants) to correct for the diamagnetic contribution. This property is then related to the system's spin for a mononuclear compound through the Curie Law⁴¹ shown in Equation 1.4, where N_A is Avogadro's number, g is the Landé g-factor for an electron ($g = 2.0023$), μ_B is the effective magnetic moment, k_B is the Boltzmann constant, T is the temperature in Kelvin, and S is the spin of the system under study. Because the HS state for Fe(II) is paramagnetic ($S = 2$), and the LS state is diamagnetic ($S=0$), the molar magnetic susceptibility product $\chi_m T$ is directly proportional to the normalised HS fraction γ_{HS} . The spin transition may then be followed by varying the temperature and measuring the change in $\chi_m T$.

$$\chi_m = \frac{N_A g^2 \mu_B^2}{3k_B T} S(S + 1) \quad (1.4)$$

1.1.2 Single crystal X-ray diffraction

The ability of single crystal X-ray diffraction to detect atomic positions with sufficiently high accuracy allows the coordination sphere around the Fe(II) centre to be seen. The difference in bond lengths between the two spin states means that, when they are available, structural data can be used to deduce the spin state of a system. Variable-temperature diffraction studies are of particular interest when coupled with magnetic studies because they can allow for the rationalisation of the magnetic properties based on the relationship that exists between the spin-active components of the lattice, as conducted via other entities in the crystal.^{42, 43} Recently, a method for assessing the intermolecular interactions within a lattice became available with the program CrystalExplorer 3.0,⁴⁴ which employs Hirshfeld surface analysis to breakdown the contacts within a crystal into a 2D fingerprint plot.⁴⁵⁻⁴⁷ This approach will be described and applied in Chapter 9. Guionneau and co-workers,⁴⁸ as well as Halcrow and co-workers,^{43, 49, 50} have published several works detailing their attempts to relate distortion within SCO compounds to the observed magnetic properties. The parameters they have used⁵¹⁻⁵³ will be introduced and discussed in Chapter 3, and especially studied in Chapter 9. Some recent advances have been made by Collet *et al.*, who have been engaged in the

study of time-resolved X-ray diffraction, to analyse how a spin crossover event is propagated throughout a system on very short time-scales after excitation.⁵⁴⁻⁵⁷

1.1.3 Differential Scanning Calorimetry (DSC)

The use of differential scanning calorimetry (DSC) first came to prominence when Sorai and co-workers used it to measure the thermodynamics of the phase transition in $[\text{Fe}(\text{NCS})_2(\text{phen})_2]$,^{58, 59} the significance of which will be described in Section 1.2. The excess heat capacity, ΔC_P , measured on varying the temperature of a sample reveals phase changes within a given compound when it undergoes SCO. Because C_P has two alternative formulations defined by Equation 1.5⁶⁰ integration of over T yields the value of the excess enthalpy, ΔH , and integration over $\ln T$ leads to the value of excess entropy, ΔS . The value of ΔS as predicted for a purely electronic transition is given by $R \ln((2S+1)_{\text{HS}}/(2S+1)_{\text{LS}})$, which for Fe(II) gives a value of $13.38 \text{ JK}^{-1}\text{mol}^{-1}$. Therefore, values above this indicate additional vibrational contributions from the lattice, with higher values associated with higher cooperativity.

$$C_P \equiv \left(\frac{\partial H}{\partial T} \right)_P \equiv T \left(\frac{\partial S}{\partial T} \right)_P \quad (1.5)$$

1.1.4 Raman spectroscopy

The bond elongation in the first coordination sphere observed on transition from the low to high spin state causes the force constants of the bonds to decrease, and so the metal-ligand stretching vibrations may be downshifted significantly.⁶¹ This opens the possibility to employ Raman spectroscopy to study SCO phenomena. As highlighted by Wolny *et al.*, although these bonds might show the greatest change in their vibrational frequencies, it is often easier to follow higher frequency bands that involve modes displayed by the coordinated ligand.⁶² A common approach has been to select a marker band, such as the CN stretching mode of coordinated thiocyanate or cyanide anions, and track its variation with temperature. As an approximation, the relative intensities of the marker peaks when the system is fully in the high or low spin state can then be used to derive a spin transition curve. A significant advantage of Raman spectroscopy with respect to other spectroscopies (Mössbauer, IR) is that it may be performed on single-crystals or powders, with no need to change the morphology of the sample.⁶³ Recently, more sophisticated

Raman studies have been used to map a spin transition over the surface of a crystal,⁶⁴ and to reversibly switch between spin states through photo-excitation.^{65, 66}

1.2 Thermodynamic considerations

The ideas and parameters outlined in Section 1.0 could be understood from a thermodynamic standpoint, which led to one of the first advances in the comprehension of SCO. To determine which of the two spin states is favoured at a given temperature under constant pressure, the expression for the change in the Gibbs free energy of the system may be used (Equation 1.6). Most immediately, the condition for $T_{1/2}$ is revealed, and corresponds to the case where the free energies of the high and low spin states are equal, *i.e.* $\Delta G = 0$, and $T_{1/2} = \Delta H / \Delta S$. Therefore, two situations can be posited: $T > T_{1/2}$ and $T < T_{1/2}$. In the former, the term $T\Delta S$ is larger than ΔH , and so the HS state is favoured. In the latter, ΔH is larger than $T\Delta S$ and the LS state is favoured.⁶⁷

$$\Delta G = G_{HS} - G_{LS} = \Delta H - T\Delta S \quad (1.6)$$

The entropically driven nature of a spin transition was revealed by Sorai and Seki. When they used differential scanning calorimetry to characterise the spin crossover of the compound $[\text{Fe}(\text{NCS})_2(\text{phen})_2]$,⁵⁹ they found $\Delta S = 48.8 \text{ JK}^{-1}\text{mol}^{-1}$,⁵⁸ which is far in excess of the value expected for the purely electronic transition ($13.38 \text{ JK}^{-1}\text{mol}^{-1}$). This excess was attributed to a coupling between the electronic states and the phonons in the lattice (elastic interactions). Thus, ΔS has two components, ΔS_{el} for the electronic change, and ΔS_{vib} for the vibrational change. The vibrational component originates in the weaker Fe-donor atom bonds in the HS state, which lead to the smaller energy differences between the vibrational modes, and higher entropy.

Attempts to simulate SCO theoretically began with the Slichter and Drickamer regular solution model.⁶⁸ For the free energy of an ensemble of N molecules where γ are in the HS state ($1-\gamma$ are LS), they introduced a factor Γ to account for the cooperativity. From this starting point, they were able to derive an expression (Equation 1.7) to link the HS fraction γ with the enthalpy and entropy changes, as well as including Γ :

$$T(\gamma) = \frac{\Delta H - \Gamma(1 - 2\gamma)}{R \ln\left(\frac{1-\gamma}{\gamma}\right) + \Delta S} \quad (1.7)$$

Simulating a spin transition curve using this expression, an appreciation may be gained for the importance of the cooperativity parameter Γ (Figure 1.4). When it is of the order of $2RT_{1/2}$, the resulting SCO behaviour is an abrupt transition (black curve). When it is

less – that is, weaker cooperativity – a gradual transition is observed (red curve). At the other extreme, when $\Gamma > 2RT_{1/2}$, then the blue curve is obtained, which corresponds to a situation with hysteresis.

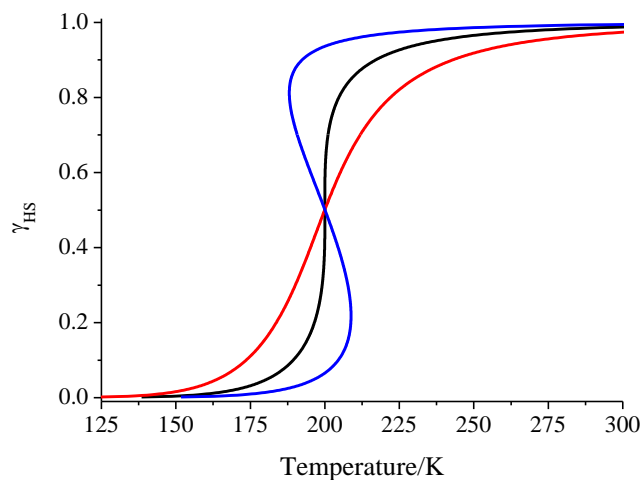


Figure 1.4: Simulations of SCO curves obtained using Equation 1.6, with $T_{1/2} = 200$ K, $\Delta H = 15$ kJ mol⁻¹, $\Delta S = 75$ JK⁻¹mol⁻¹, and $\Gamma = 1500$ (red), 3340 (black), 5100 Jmol⁻¹ (blue).

This regular solution model is so-called because its authors proposed that the low and high spin centres were arbitrarily distributed over the lattice. In contrast, Sorai and Seki introduced the important concept of domains, where molecules of like spin are grouped together in the lattice.⁶⁹ The smaller the domains, the less abrupt the transition. The problem encountered with their model was that it couldn't account for hysteresis. However, both models, proposed in the early 1970s, have been the essential starting point for the subsequent development of theory in the field.^{70, 71}

1.3 Trapping of meta-stable high spin states

The study of cooperative effects in SCO systems was facilitated by one of the major developments in the field. While McGarvey initially observed for a series of compounds that in solution a HS population could be generated by exciting the LS state using a pulsed laser,⁷² Decurtins and co-workers performed the experiment at cryogenic temperatures in the solid state on the compound [Fe(ptz)₆](BF₄)₂ (ptz = 1-propyltetrazole) and described how the relaxation back to ground LS state slowed sufficiently to enable trapping of the sample in a metastable high spin state.^{73, 74} This phenomenon was called Light Induced Excited Spin State Trapping (LIESST). The same group then achieved the

reverse-LIESST effect – re-population of the LS state by irradiating the metastable HS state – by changing the wavelength of light used to irradiate the same compound.^{75, 76} The mechanism for the LIESST and reverse-LIESST effect is shown on the left in Figure 1.5.⁷⁷ For LIESST, irradiation excites a LS centre to the 1T_1 state. There are then two fast, non-adiabatic intersystem crossing steps, passing through 3T_1 and populating the HS 5T_2 state. Here, the large difference in Fe-donor atom bond lengths between the high and low spin states together with the small ΔE_{HL}^0 creates a barrier to relaxation, and so the system remains trapped. An alternative trapping method is by rapid or flash cooling.⁷⁸ For this technique, the SCO system is quickly inserted into a given apparatus which has been pre-cooled to very low temperatures. This trapping, Thermally Induced Excited Spin State Trapping (TIESST) doesn't involve the intersystem crossing steps outlined above, because it essentially freezes in the high temperature HS phase. The isothermal relaxation mechanism is still the same, and so the following discussion still applies.

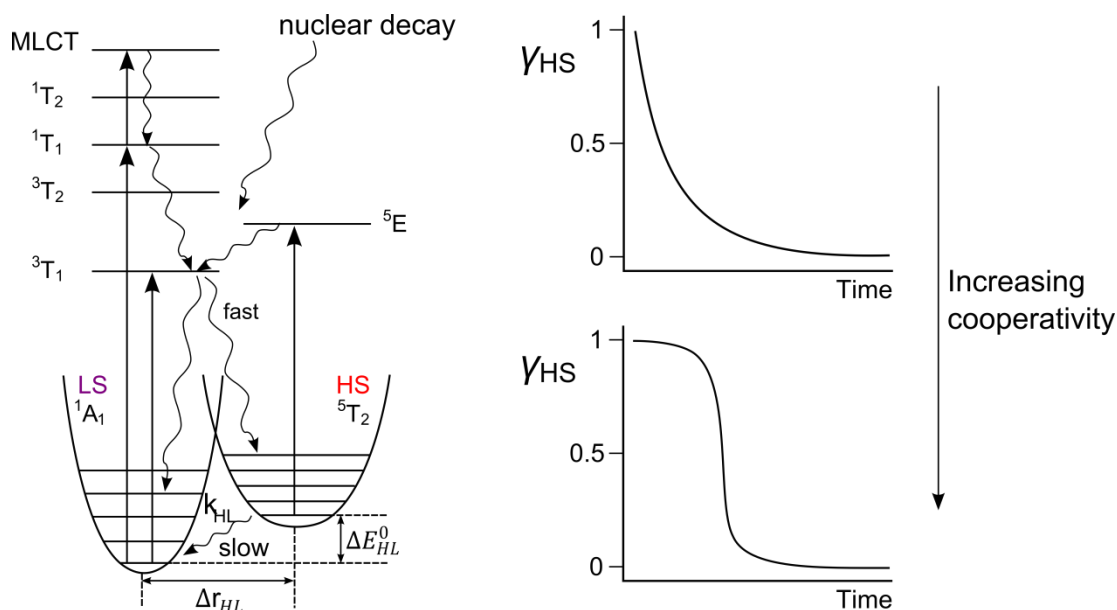


Figure 1.5: (left) Potential wells and mechanism for excitation and relaxation in a LIESST experiment. Adapted from reference 77. (right) Two discussed types of relaxation curves, see the text for details.

To observe the relaxation, the system can be trapped at a given temperature, and the isothermal high spin fraction's dependence on time measured (Figure 1.5, right).⁷⁹ At very low temperatures the only available mechanism for the system to relax is by quantum mechanical tunnelling, while at higher temperatures the relaxation is thermally activated. The cooperativity of the trapped system plays an important role in how the

relaxation process occurs, and two cases – high and low cooperativity – may be considered. When a system is lowly cooperative, the relaxation kinetics are first-order, and are described by the expressions 1.8 and 1.9:

$$\gamma_{HS} = \exp(-k_{HL}(T)t) \quad (1.8)$$

$$k_{HL}(T) = k_{\infty} \exp\left(\frac{-E_a}{k_B T}\right) \quad (1.9)$$

Following Equation 1.8, the temporal evolution of the HS fraction is simply an exponential decay, with the rate dependent only on the temperature.⁷³ By performing a series of isothermal kinetics experiments at different temperatures, the resulting relaxation curves may be fitted to obtain the corresponding values of k_{HL} . An Arrhenius plot of Equation 1.9 can then be used to derive the activation energy of the relaxation process as well as k_{∞} . Highly cooperative systems usually present sigmoidal relaxation curves⁸⁰ and require the equations to be adapted:⁸¹

$$\left(\frac{\partial \gamma}{\partial t}\right) = -k_{HL}(T, \gamma_{HS}) \gamma_{HS} \quad (1.10)$$

$$k_{HL}(T, \gamma_{HS}) = k_{HL}(T) \exp[\alpha(T)(1 - \gamma_{HS})] \quad (1.11)$$

$$k_{HL}(T) = k_{\infty} \exp\left(\frac{-E_a}{k_B T}\right), \alpha = \frac{E_a^*}{k_B T}$$

These adjustments are necessary to account for the self-accelerating behaviour reflected by the shape of the curves. Firstly, Equation 1.10 is a differential equation with no analytical solution, needed because the rate of relaxation k_{HL} is no longer solely dependent on the temperature, but now also on the high spin fraction, γ_{HS} . This relaxation rate can be split into two components (Equation 1.11), one which corresponds to the temperature dependent relaxation rate of Equation 1.9, and another that introduces the parameter α , due to the high cooperativity.⁷⁷ The self-acceleration behaviour can be understood by considering the volume difference between the high and low spin centres. When the system is fully trapped in the metastable HS state, the energy difference between the potential wells of both states is small, corresponding to the original ΔE_{HL} . As the LS population begins to grow within the lattice, the denser singlet state creates an internal pressure, which destabilises the HS state, shifting its potential well to higher energy. This destabilisation depends on the LS population, which is continually increasing with the relaxation process, and causes the increase in the rate of relaxation.

The thermal limit of these bi-stable domains at low temperature is defined by $T(\text{LIESST})$ (or $T(\text{TIESST})$, analogously for the thermal trapping experiment).⁸² This

value is obtained by trapping the system and warming it slowly until it relaxes to the LS state. The minimum of the derivative of the HS→LS curve yields the value of $T(\text{LIESST})$. Létard and co-workers compiled a database of the $T(\text{LIESST})$ values found in the literature, and compared them with their partner $T_{1/2}$ values,⁸³ to obtain the plot shown in Figure 1.6. They found that the compounds displayed a tendency consistent with the straight line Equation 1.12. The value of T_0 depends on the denticity of the ligand, and the value of $T(\text{LIESST})$ is inversely proportional to $T_{1/2}$. This last finding is consistent with the inverse energy gap law, which dictates that the HS→LS relaxation is directly dependent on the zero point energy gap ΔE_{HL}^0 .^{84, 85} This means that the larger this gap, the less stable the meta-stable HS state, and the relaxation is produced at lower temperatures. It also means that the compound must be raised to higher temperatures in order to populate the HS state.

$$T(\text{LIESST}) = T_0 - 0.3T_{1/2} \quad (1.12)$$

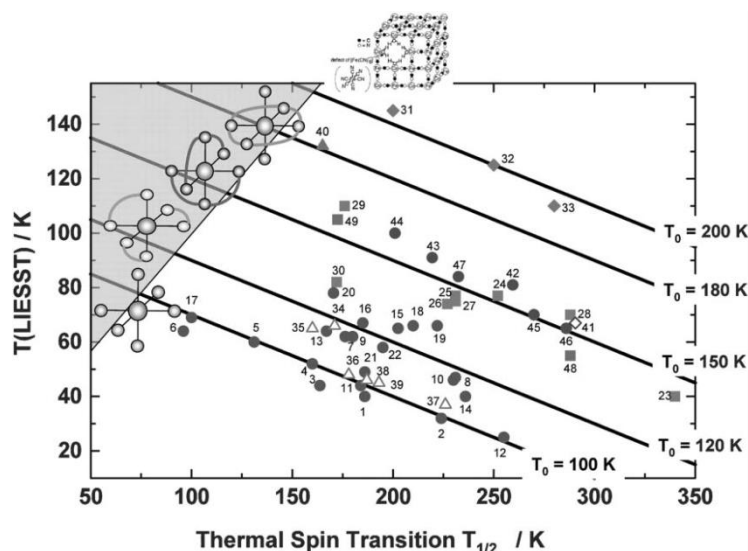


Figure 1.6: Correlation between $T(\text{LIESST})$ and $T_{1/2}$ as compiled in reference 83. The grey region indicates the impossible overlap of the two values.

1.4 Latest advances and applications

The interest in SCO and the extent of research effort being expended is reflected by the way in which advances are occurring in all areas of the field. This year, a cluster issue of European Journal of Inorganic Chemistry dedicated to SCO had to be expanded to two issues, to cover the work in which research groups are engaged.⁸⁶ Together with the original research papers included in that double issue, eight microreviews were included to discuss many aspects from this increasingly deep line of science. And that is not to

mention a recent review by Roubeau on SCO coordination polymers,⁸⁷ an extended overview of the field by Garcia,³⁹ and the monograph published this year edited by Halcrow, “Spin-Crossover Materials: Properties and Applications”.⁸⁸ Therefore, the aim this section is to highlight the feedback loop that exists between synthetic chemists and physical chemists, whereby increasingly sophisticated chemical systems are subject to increasingly sophisticated physical studies and applications.

1.4.1 Beyond bi-stability

While the spin transition curves presented in Figure 1.3 allow for, at most, the bi-stability that is inherent to a standard hysteresis loop, there have been some recent examples of multi-stable systems. The compound $[\text{FeL}(\text{CN})_2] \cdot \text{H}_2\text{O}$, where L was a macrocyclic ligand occupying the equatorial plane of the Fe(II) ion’s coordination sphere, as studied by Costa and co-workers was shown to display three different possible phases at low temperatures.^{89, 90} The HS form of the complex was found to contain a heptacoordinated metal centre where the five equatorial positions of the Fe(II) ion are occupied by donor atoms from the macrocyclic ligand. The spin crossover caused a reversible bond breaking between the macrocycle and Fe(II), such that the LS form was hexacoordinate. Below 125 K, the compound could be found in a majority LS state; in another it displayed a 1:1 distribution of HS:LS molecules; and in a third photo-excited phase it proved to have a majority HS population.

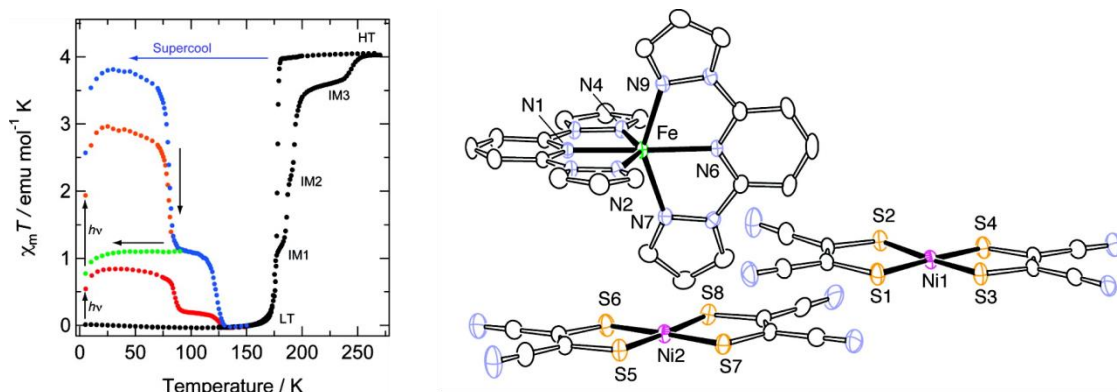


Figure 1.7: (left) The magnetic properties of the compound $[\text{Fe}(1\text{-bpp})_2][\text{Ni}(\text{mnt})_2]_2$. (right) The molecular structure of the compound. Taken from reference 91.

While the meta-stability of the previous compound was intrinsic to the Fe-based molecule, a mononuclear compound based on the ligand 2,6(pyrazol-1-yl)pyridine (1-

bpp) was coupled with the anion $[\text{Ni}(\text{mnt})_2]^-$, and complex $[\text{Fe}(1\text{-bpp})_2][\text{Ni}(\text{mnt})_2]_2$ was shown to possess five different phases at low temperature, as well as three intermediate phases between the low and high spin states in the heating mode (Figure 1.7).⁹¹ In the high temperature regime, the compound is fully HS and slow cooling induces a first order transition to the fully LS phase. This process also entails the dimerisation of the anions, leading to the fully diamagnetic state. In the heating mode, the return to the HS state has four steps. In the first, 1/3 of the Fe(II) ions convert to the HS state, and in the second, an additional 1/3 convert, such that the phase IM2 contains a 2/3 HS population and dimeric Ni(II) moieties. The third step sees the remaining LS Fe(II) ions become HS, and one of the two Ni(II) dimers separates. The final step involves the separation of the other Ni(II) dimer, returning the system to its maximum χT value. The four additional low temperature phases could be obtained thus: the first by irradiation of the LS phase, leading to a partial excitation to a photo-excited state (red dots). The second involves flash cooling of the HS sample to 10 K (blue dots), and it is from this phase that the remaining two may be generated. The third is obtained by allowing only the partial relaxation of the supercooled phase (yellow dots), and by cooling from here and irradiating, the fourth phase may be achieved (orange dots). A three-step switch from the LS state back to the HS state was also recently described in a 3D system based on the Hoffman Clathrates, although in that case, the plateaus associated with each intermediate spanned a wider temperature range.⁹²

1.4.2 Physical control of domains

In the last six years, the SCO compound $[\text{Fe}(\text{bapbpy})(\text{NCS})_2]$ (bapbpy = N6,N6'-di(pyridine-2-yl)-2,2'-bipyridine-6,6'-diamine) has become one of the most intensively studied in the field. The molecular structure and variable temperature magnetic properties are shown in Figure 1.8. The compound displays a two-step transition, and both steps are associated with hysteresis loops.^{64, 93} The exact nature of these transitions were found to depend on the sample preparation, although the most abrupt phenomena were observed for single crystal samples.⁹⁴ The compound was subject to extensive crystallographic investigation. This initially led to the conclusion that the intermediate phase of the compound displayed crystallographic ordering of the high and low spin sites, of the type [HS-LS-LS].⁹⁴ Shepherd and co-workers have since made two remarkable contributions to the understanding of this system. In the first, they tracked the SCO with pressure:

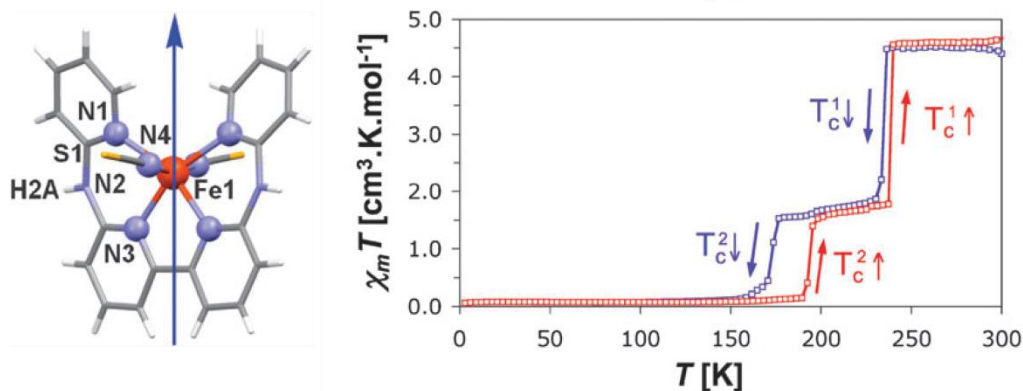


Figure 1.8: (left) The molecular structure of the complex [Fe(bapbpy)(NCS)₂] and (right) its variable temperature magnetic properties. Both figures taken from reference 94.

crystallographically, magnetically, and with Raman spectroscopy.²⁴ This was then followed by a paper where the compound was shown to display four distinct metastable states.⁹⁵ These states could be generated by LIESST of the fully LS phase (I), the partial relaxation of I to yield a metastable intermediate phase (II), a thermally quenched intermediate phase (III), and finally a LIESST phase formed by irradiation of III (IV).

At the same time, Bedoui *et al.* used optical microscopy combined with Raman spectroscopy to characterize the nucleation of the spin crossover process of this compound in the single crystals.⁶⁴ By using Raman mapping the authors of that study were able to follow the propagation of the first transition, which was shown to proceed in a single direction along the length of the crystal, and was therefore attributed to a unique domain. The second transition to the fully LS state was shown to be somewhat more complex, and associated with several domains. The relatively simple changes observed in the first transition were therefore ideal for their subsequent attempt to control the propagation of the spin crossover via “domain engineering”.^{96,97} Figure 1.9 (a) shows the crystal initially in the fully HS state (red), with the natural origin of the transition’s propagation indicated by the triangle. As the temperature is decreased (left to right) the compound switches to the intermediate phase (blue), approximately from the top of the crystal to the bottom. In their first attempt to control the domain propagation (Fig. 1.9 (b)), a defect was generated by laser ablation in the centre of the crystal (indicated by the square). Although the subsequent cooling showed a slight emanation of the transition from this defect, the dominant propagation was that originally observed in a. For the introduction of the second defect, they changed position within the crystal and increased the energy of the laser pulse used. The success of this approach is shown in Figure 1.9 (c),

where the propagation is shown to begin with the defect, and the original propagation is suppressed. Therefore, using this ablation method, the authors were able to control the direction of the domain propagation in a SCO material.

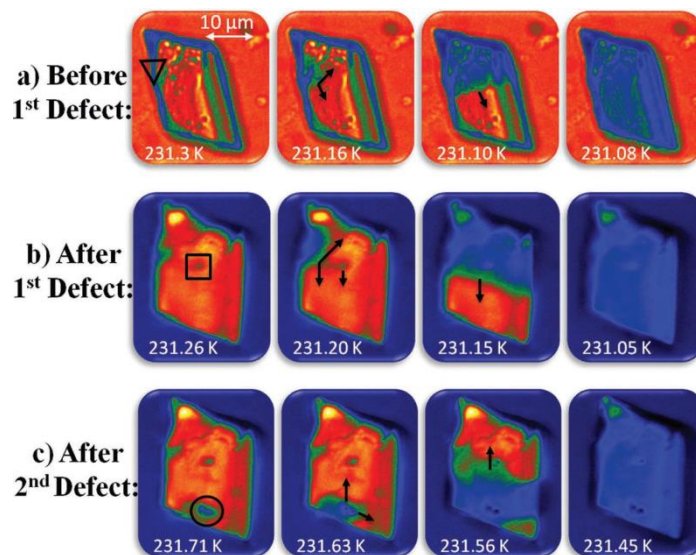


Figure 1.9: Optical microscopy images taken of $[\text{Fe}(\text{babpy})(\text{NCS})_2]$ in bright field. The red colour represents the fully HS phase, blue the intermediate phase. Taken from reference 96.

1.4.3 Size reduction

In the 1990s, Kahn proposed SCO polymers based on triazole ligands, of the general formula $[\text{Fe}(\text{trz})_3]\text{X}_2$ where trz represents a given triazole derivative and X a counter-ion, as candidates for memory devices or temperature sensors.^{98, 99} The foundation of this suggestion was the combination of the colour change in these systems, which is often a clear purple to white on switching from LS to HS, and the frequent occurrence of hysteresis loops. Létard and co-workers reported an early attempt to use this family of compounds as the switching component in nanoparticles, resulting in clusters of the compound $[\text{Fe}(\text{NH}_2\text{trz})_3]\text{Br}_2$ with a size limit of between 60 and 200 nm.¹⁰⁰ A landmark paper by Coronado and Galán-Mascarós subsequently described the preparation of SCO nanoparticles with hysteresis using a related triazole ligand, at the same time taking a qualitative jump in size-reduction to an average particle size of less than 20 nm (Figure 1.10).¹⁰¹ Their nanoparticles of $[\text{Fe}(\text{Htrz})_2(\text{trz})](\text{BF}_4)$ (Htrz = 1,2,4-*H*-triazole) were found to be bi-stable over a broad temperature range, and a hysteretic response was observed (although reduced to ~30 K) on further size reduction to 6 nm particles.¹⁰²

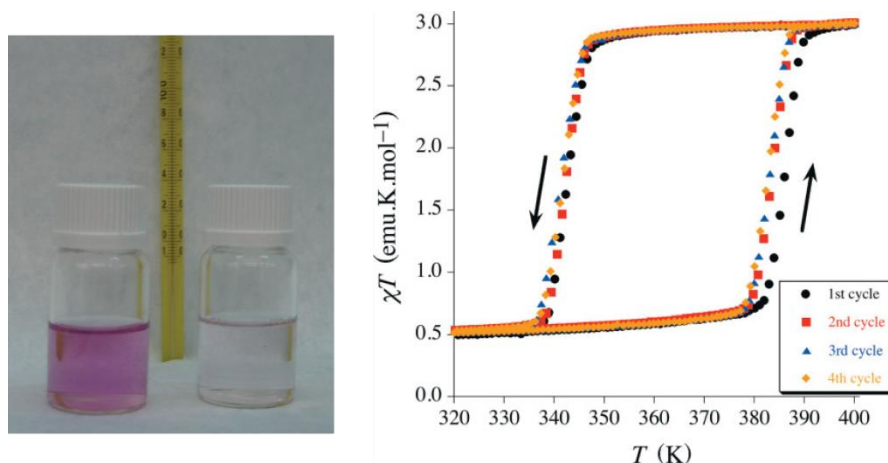


Figure 1.10: (left) Stable suspensions of nanoparticles of $[\text{Fe}(\text{Htrz})_2(\text{trz})](\text{BF}_4)$ in their two different spin states at the same temperature. (right) The magnetic susceptibility of the nanoparticles on performing several temperature cycles. Figures taken from reference 101.

In a later work, these particles were deposited between two Au electrodes, and demonstrated to display bi-stability of conductance on varying the temperature.¹⁰³ This investigation was performed by the group of van der Zant, who subsequently published a combined theoretical and experimental study that moved away from nanoparticles, to single molecules. In that article, gas phase calculations were used to predict the possible spin switch of a single molecule, $[\text{Fe}(\text{L})_2]^{2+}$ where $\text{L} = 4'-(4''''\text{-pyridyl})-1,2' :6'1''\text{-bis}(\text{pyrazolyl})\text{pyridine}$, as induced by the charging of the ligand by an electric field.¹⁰⁴ An

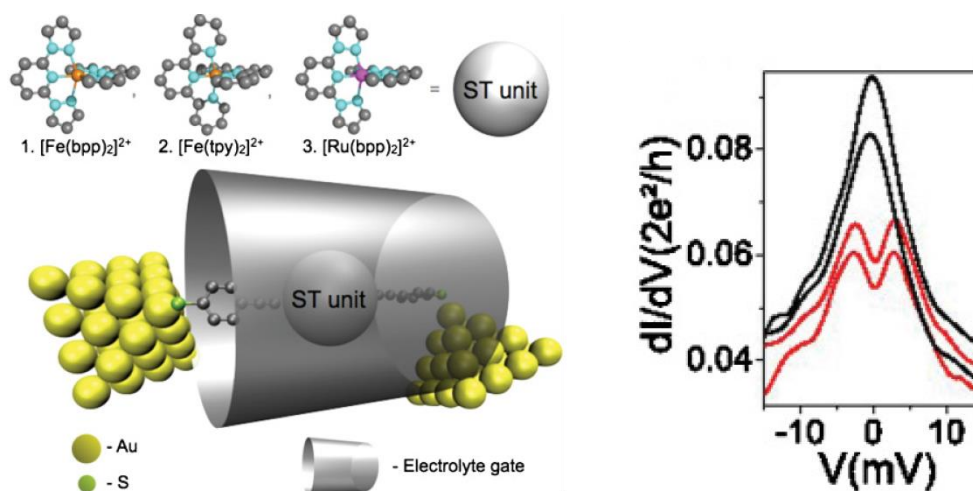


Figure 1.11: (left) A schematic representation of the three-point device that connects two electrodes to two different points of a given single molecule and the molecule to an external gate. (right) The differential conductance for a mononuclear Fe(II) complex vs. the source-drain voltage at 2, 2.4, 2.9, and 3.3 V (top to bottom). Taken from reference 104.

idealisation of the device used to perform this switch is shown in Figure 1.11. The molecule, through some extended ligand, is connected at one end to the source and at the other to the drain electrodes, and is electrostatically coupled to an external gate. According to the theory, the switch between spin states would be manifested as a split in the differential conductance at zero-bias. This was observed in the traces shown in the Figure. As the gate voltage is increased, from 2, through to 2.4, 2.9, and 3.3 V, the differential conductance vs. source-drain voltage is seen to split. The authors of the paper highlighted that although their interpretation is supported by the theoretical study they provide, further experiments are still needed to be able to definitively attribute this splitting to a spin transition.

1.4.4 Detection of SCO on increasingly small scales

The challenge apparent in the previous system is that of how to unequivocally detect spin crossover as the size of the studied objects becomes increasingly small. The development of new physical methods that can probe the spin switch is therefore of paramount importance. A recent contribution by the group of Bousseksou proposed the variation in surface plasmon polariton waves (SPPs) as a possible means of observing spin crossover in thin layers (30 nm) of a spin transition polymer $[\text{Fe}(\text{hptrz})_3](\text{OTs})_2$ (hptrz = 4-heptyl-1,2,4-triazole, and Ots = tosylate).¹⁰⁵ At the interface between a dielectric material and a metal, light irradiation can induce the propagation of SPPs. The use of a fixed wavelength should lead to surface plasmon resonance at a given angle, θ_{SPR} , with its exact value dependent on the nature of the dielectric layer. The authors were able to observe a hysteretic response in the nanolayers manifested as a shift in θ_{SPR} as they varied the temperature and therefore spin state of the polymeric material.

In an article published this year, the same group provided nanoparticles of the same polymer for use in a prototype micromagnetometer.¹⁰⁶ The aim of the study was to demonstrate the ability of a magnetoresistive device to measure the spin switch in extremely small particles (those used in the study had a diameter of 250 nm, and the volume of the aggregate measured was $\sim 3 \times 10^{-3} \text{ mm}^3$), and at room temperature. Figure 1.12 shows the change in voltage of the micromagnetometer induced by the change in spin state of the particles with varying temperature. The normalised reflectance of the particles on the surface was also followed, and shown to corroborate the voltage output observed of the device.

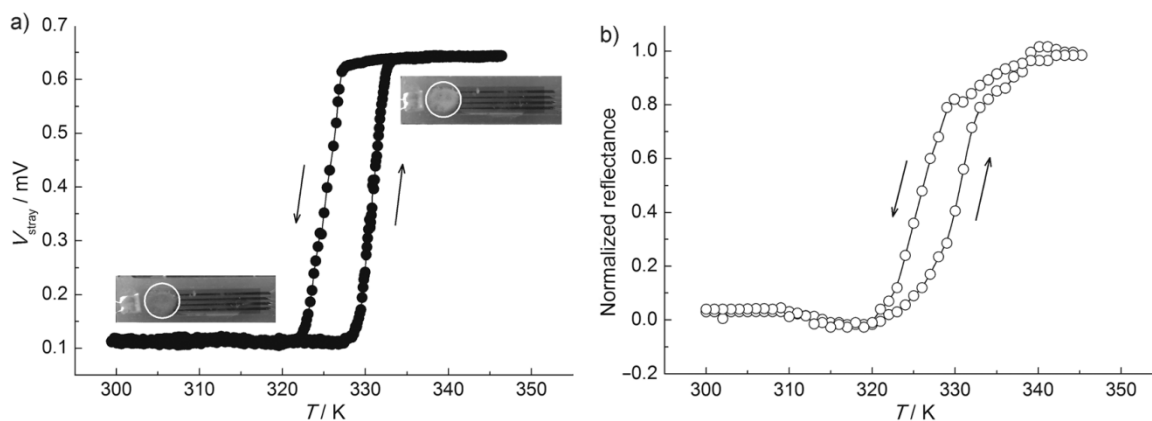


Figure 1.12: (left) The variation in voltage with temperature caused by the nanoparticles $[\text{Fe}(\text{hptrz})_3](\text{OTs})_2$ in a prototype micromagnetometer. (right) The normalised reflectance of the particles on varying the temperature, as obtained from the nanoparticles on the device. Taken from reference 106.

1.4.5 SCO materials as fluorescent thermometers

In a series of recent papers, the groups of Bousseksou and Colacio have separately outlined strategies to combine the switching properties of SCO nanoparticles with the fluorescent properties of external molecules as a way of creating multifunctional materials that serve as fluorescent thermometers. The principle of these studies lies in the overlap of the fluorophore's emission spectrum with the absorption band of one of the two spin states of the Fe(II) system. When this occurs, the emission of the fluorophore may be partially quenched. Therefore, by changing the spin state, the fluorescence emission can

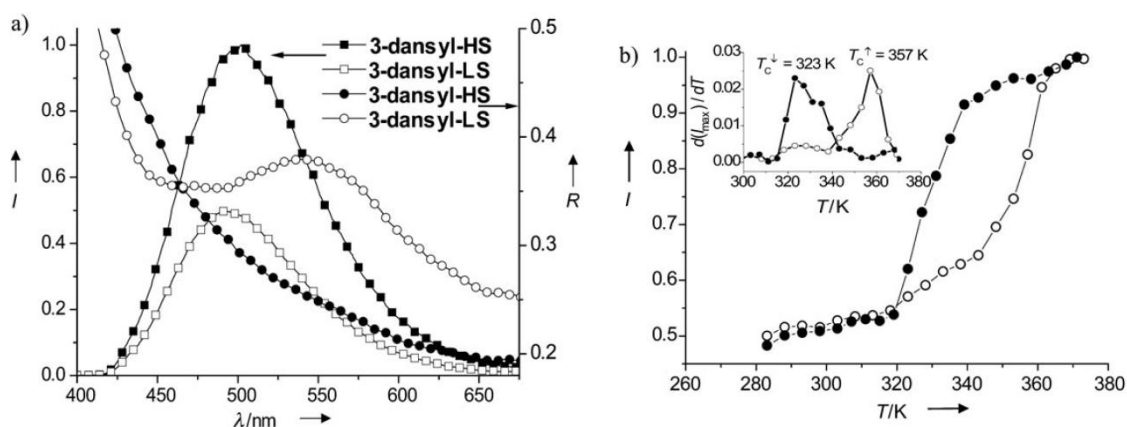


Figure 1.13: (left) The diffuse reflectance (R) and fluorescence (I) of $[\text{Fe}(\text{Htrz})_2(\text{trz})](\text{BF}_4)$ nanoparticles doped with 3-dansyl. (right) The variation of fluorescence intensity at 495 nm on changing the temperature. Taken from reference 107.

be modulated between “on” and “off”. To achieve this, both groups chose to dope nanoparticles of Fe(II) triazole polymers with fluorescent molecules. The work published by Colacio *et al.* used silica-based nanoparticles of $[\text{Fe}(\text{Htrz})_2(\text{trz})](\text{BF}_4)$, with silica chosen for its high porosity, and doped them with the molecule 3-(dansylamido)propyltrimethoxysilane.¹⁰⁷ Figure 1.13 (a) presents the diffuse reflectance (R) and fluorescence (I) for a Zn/Fe 1:1 hybrid polymer on silica that was doped with the fluorophore at 280 K and 400 K, which correspond to the low and high spin regimes, respectively. The variable temperature fluorescence measurements (Figure 1.13 (b)) show how the response of the system may be altered as a function of the spin state.

In the Bousseksou group’s initial study, they employed $\text{Fe}(\text{NH}_2\text{trz})_3(\text{OTs})_2$ nanoparticles, and doped them with rhodamine110 molecules (Rh110).¹⁰⁸ First, they demonstrated the temperature dependence of the fluorescence intensity of the nanoparticles around room temperature. The next step taken was to deposit the suspension of the material on nickel nanowires. The temperature of the wires can be efficiently varied by applying a DC current. Thus, the system could be switched between the “on” and “off” states by flipping between an applied current of 6 mA and 0 mA, respectively (Figure 1.14). The flow of current through the wires induces a jump in the temperature, transmitted to the Fe(II) nanoparticles, which then change to the HS state. The polymer then no longer quenches the emission of the Rh110 molecules, and fluorescence microscopy was used to observe the glowing nanowires. In a subsequent paper, they were able to take a related polymer doped with acridine orange, and create ordered arrays of SCO nanodots.¹⁰⁹

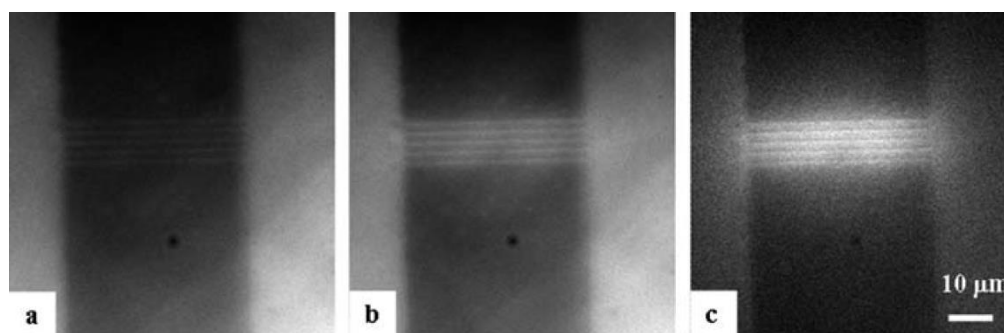


Figure 1.14: Thermal imaging of $\text{Fe}(\text{NH}_2\text{trz})_3(\text{OTs})_2$ coated nanowire heaters. (a) Corresponds to no external bias, (b) under the application of an external bias of 6 mA, (c) is the subtraction of (a) from (b). Taken from reference 108.

What the above steps in SCO research come to represent is the intense interest that exists for these systems, and the inter-disciplinary approach required to innovate within the field. While increasingly *physical* studies look to take advantage of the characteristics of SCO materials, whether by using them as fluorescence thermometers, as a means of testing cutting edge prototypes for micro-magnetometers, or by using their molecular structure as a means for placing them between electrodes, the first step still involves *synthetic* chemistry to provide the systems. The synthesis of the molecule [Fe(babpy)(NCS)₂] and the perfection of its crystallisation conditions then allowed the Bousseksou group to physically control the domain propagation within the crystals. The size reduction of the SCO objects as developed by Létard and Coronado amongst others, as well as the bispyrazolyl based SCO cation provided by Ruben, then permitted the Van der Zant group to place these nano-objects between electrodes. Therefore, the role of the synthetic chemist is to continue to devise and create suitable chemical entities. A promising family of candidate compounds is based on the polypyrazolyl ligand 3-bpp, which will be described in the following section.

1.5 2,6-Bis(pyrazol-3-yl)pyridine

Although the synthesis of the polypyrazolyl ligand 2,6-bis(pyrazol-3-yl)pyridine (3-bpp) had been described in 1977,¹¹⁰ its first application in the field of SCO came in 1987/1988, with two papers by Sugiyarto and Goodwin (Figure 1.15).^{111, 112} They described the variable temperature magnetic properties of a series of Fe(II) compounds containing various pyridine-substituted pyrazole ligands, amongst which those of 3-bpp proved to be the most interesting. The system [Fe(3-bpp)₂](BF₄)₂ displayed a thermal spin transition with a 10 K hysteresis loop centred around 175 K. In contrast, the dihydrate of this salt, [Fe(3-bpp)₂](BF₄)₂·2H₂O, presents a far more gradual spin crossover with $T_{1/2} = 300$ K. The authors suggested that the differences observed in the magnetic behaviour could be attributed to the effect of the hydrogen bonding in which the water molecules would participate within the lattice, and tentatively proposed that in the anhydrous salt there would be more direct “communication” between the cations, leading to the more cooperative spin transition. Unfortunately, no single crystal X-ray diffraction data could be collected for these compounds, although the powder diffractograms showed that they were associated with distinct crystallographic phases. In a subsequent article, the authors extended their studies to encompass a greater range of charge-balancing anions to

accompany the same divalent cation, and achieved the first resolution of the crystal structures associated with these compounds.¹¹⁴ They were able to crystallise the system $[\text{Fe}(\text{3-bpp})_2](\text{BF}_4)_2 \cdot 3\text{H}_2\text{O}$, and were able to demonstrate the interaction between the pyrazolyl moieties and either the water molecules in the lattice or the tetrafluoroborate anions. The bulk magnetic properties of this trihydrate were not measured, but the observed Fe-N bond lengths were indicative of LS cations at room temperature.

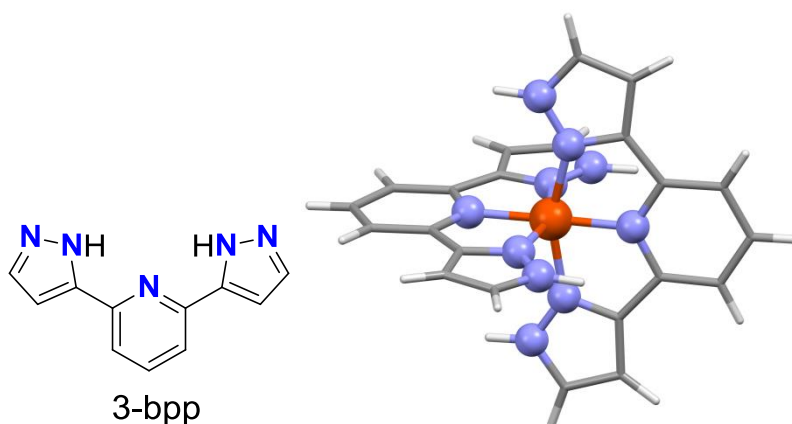


Figure 1.15: The polypyrazolyl ligand 3-bpp, and its typical mode of coordination, shown for the compound CAZJET.¹¹³

A more dramatic manifestation of these solvation-dependent magnetic properties was found in the triflate salts of the same cation, $[\text{Fe}(\text{3-bpp})_2](\text{CF}_3\text{SO}_3)_2 \cdot n\text{H}_2\text{O}$ ($n = 0,1,3$). The LS trihydrate could be heated to induce the release of two water molecules, and bring about the formation of the stable monohydrate, which was shown to be HS at room temperature. Variable temperature magnetic and Mössbauer measurements performed on the monohydrate were then used to demonstrate the existence of an abrupt quintet to singlet transition around 145 K (Figure 1.16).¹¹⁵ On heating the sample, the magnetic response diverged from that found in the cooling branch, and initially showed a less abrupt, partial transition to a plateau corresponding to around 35% of the Fe(II) centres in the HS state. Continued heating brought about a more abrupt return to the fully HS state from this mixed population. This two-step recovery of the quintet state therefore presents a hysteresis loop that spans a bi-stable region of 140 K at its widest point. The relaxation kinetics of the metastable states of the monohydrate were also characterised. It was found that the relaxation mechanism associated with the trapped cations differed, depending on whether the metastable state had been thermally generated via flash cooling or photo-induced by irradiation of the LS state. Again, a rationalisation of these properties on the

basis of the crystal structure was hampered by the lack of data. The structure was later elucidated for the LS trihydrate, and the Fe-N distances around the Fe(II) ion found to be in agreement with the magnetic measurements. Of the four potential hydrogen bonding donors on the pyrazolyl rings, three were seen to form interactions with water molecules, with the remaining N-H group left to interact with the triflate anion. A study of the spin crossover properties of the compound $[\text{Fe}(\text{3-bpp})_2](\text{BF}_4)_2$ in solution concluded that hydrogen bonding of water molecules stabilised the LS state of the system, evidenced by a shifting of transition temperature to higher values of $T_{1/2}$ on increasing the proportion of water in the solvent mixture.³²

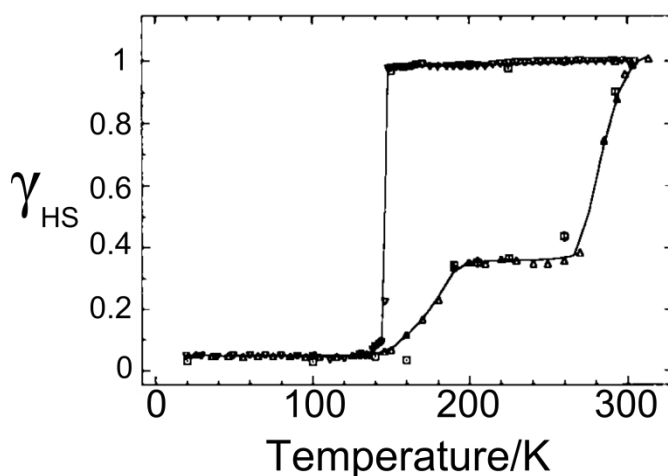


Figure 1.16: The variable temperature magnetic properties of the compound $[\text{Fe}(\text{3-bpp})_2](\text{CF}_3\text{SO}_3)_2 \cdot \text{H}_2\text{O}$. Taken and modified from reference 115.

This appreciation of the sensitivity of the 3-bpp compound's magnetic properties to hydration has been extended to studies of the LIESST-generated metastable states of the $[\text{Fe}(\text{3-bpp})_2](\text{X})_2 \cdot n\text{H}_2\text{O}$ family. Marcén and co-workers took this family of complexes as the basis of an investigation into how the degree of hydration affects $T(\text{LIESST})$.¹¹⁶ Because the cation of the eight complexes they irradiated was the same, they considered the bi-stable domains encountered as independent of the changes to the inner coordination sphere. Therefore, the effect of entities that lie outwith the first coordination sphere (anions, lattice water molecules) on $T(\text{LIESST})$ could be analysed. This study led to the inclusion of a further trend-line in the correlation shown in Figure 1.6, corresponding to tridentate ligand systems. Six of the eight compounds were found to have $T(\text{LIESST})$ values within a range of 70 to 82 K, while at the same time displaying $T_{1/2}$ values spanning from 168 K to 288 K. They concluded that while the thermal magnetic

properties (characterised by $T_{1/2}$) are highly sensitive to the hydration and anion associated with the cations, the same cannot be said of the T_0 .

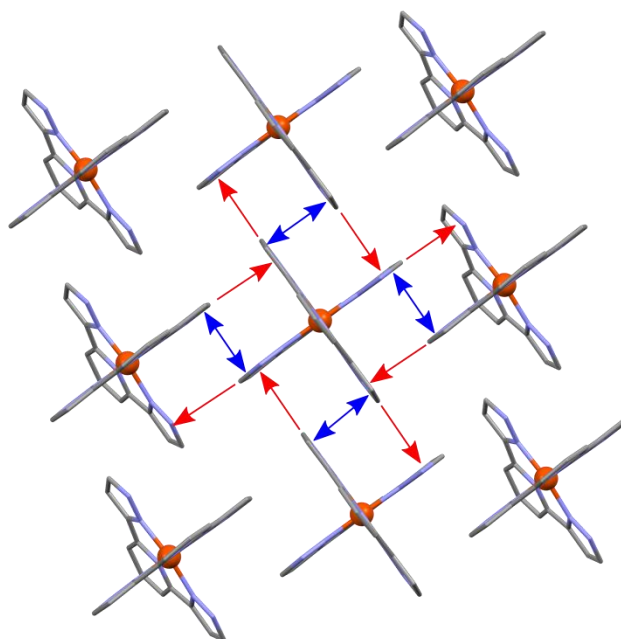


Figure 1.17: Illustration of the terpyridine embrace, as present in CAZJET.¹¹³ Hydrogen atoms have been omitted for clarity. The double-headed blue arrows correspond to $\pi \cdots \pi$ contacts, while the single-headed red arrows correspond to $C-H \cdots \pi$ interactions.

The notable scarcity of crystal structures for these systems meant that many of the proposed justifications for the observed magnetic properties were merely speculative,¹¹⁷ based on the intuition that the shape of the $[Fe(3-bpp)_2]^{2+}$ cation, with the planar nature of the chelating species and the availability of hydrogen donor motifs, would encourage interaction with the anion and the solvent molecules in the lattice. As more structures were obtained, the favoured packing motif of these systems was found to be based on the face-to-face overlap of aromatic rings on neighbouring cations, with the interaction reinforced by edge-to-face $C-H \cdots \pi$ contacts conducted by the pyrazolyl rings (Figure 1.17).^{113, 118-121} This combination of intermolecular interactions was found to induce the cations to form co-planar arrays, with the hydrogen bonding groups pointing away from these planes. Scudder and co-workers demonstrated this motif to be predominant in compounds of the general formula $[M(L)_2]$ where L is an aromatic tridentate ligand, and the complex displays meridional octahedral stereochemistry.^{119, 122} They detailed this packing in the compound $[Co(terpy)_2]^{2+}$ complex, and hence the arrangement is called the “terpyridine embrace”. Consequently, through the synthesis of approximately “cross”-

shaped cations, this disposition of the lattice components may be favoured, with the relationship between each cation modulated through the use of differing solvents, and variation of the charge-balancing anion.

A version of this packing motif was observed in a recent article concerning the spin crossover properties of the compound $[\text{Fe}(\text{3-mbpp})_2](\text{BF}_4)_2$ (3-mbpp = 2,6-bis(5-methylpyrazol-3yl)pyridine).¹²³ The authors indicated that the steric bulk of the distal methyl groups impeded a more efficient overlap between the faces of the neighbouring pyrazole rings. In the freshly prepared compound, which presents the composition $[\text{Fe}(\text{3-mbpp})_2](\text{BF}_4)_2 \cdot 2\text{H}_2\text{O}$, half of the Fe(II) ions are in the HS state, a situation maintained when cooling from 200 K. However, when the sample is heated, there is a reversible partial transition of the LS centres to HS between 200 and 300 K, reflected by an increase in the molar magnetic susceptibility (Figure 1.18). Continued heating to 350 K causes the release of the water molecules, and yields the anhydrous salt, with a concomitant jump in χT corresponding to a full HS population. A thermal cycle of this anhydrous phase reveals a hysteresis loop that is 37 K wide. Further investigation of the anhydrous compound showed it to be associated with five different crystallographic phases. Starting from the hydrated salt, the compound could be heated to induce desolvation of the sample and yield HS phase B at 353 K. Cooling B to 303 K caused a phase transition to HS phase C, with further cooling to 268 K bringing about the formation of HS phase D. This phase D

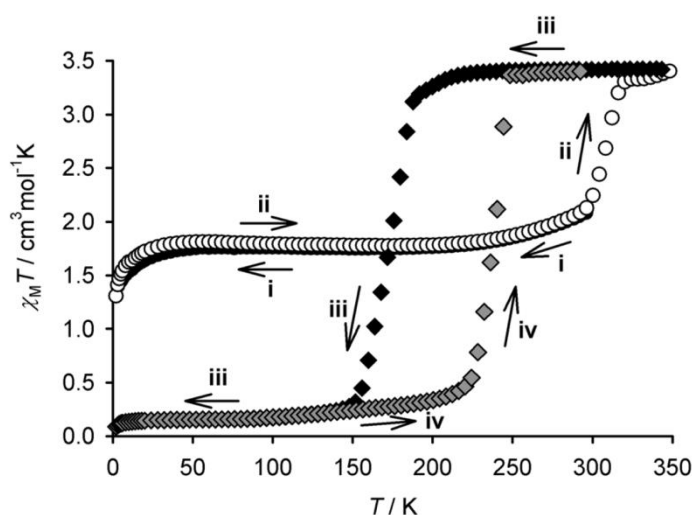


Figure 1.18: The variable temperature magnetic properties of the compound $[\text{Fe}(\text{3-mbpp})_2](\text{BF}_4)_2$.

The various heating and cooling modes, and concomitant chemical changes are described in the text. Taken from reference 123.

is then that which undergoes the hysteretic spin transition that leads to LS phase E. The fifth anhydrous phase, A, was obtained occasionally on crystallisation of the high temperature HS phase. This phase was very hygroscopic, preventing the measurement of its bulk magnetic properties, although the single crystal X-ray structures resolved for this phase at 300 and 150 K showed the system to be fully in the HS and LS states, respectively.

By employing topologically more complex anions,¹²⁴ Coronado *et al.* could synthesise a series of compounds that necessarily imposed an ordering in the crystal lattice distinct to the terpyridine embrace. They used the anionic complex $[\text{MnCr}(\text{ox})_3]^-$ in their attempt to obtain a multifunctional material that would combine the SCO properties of the $[\text{Fe}(\text{3-bpp})_2]^{2+}$ cation with magnetic ordering within the 3D polymeric structure of the anion.¹²⁵ The structure of the synthesised compound, $[\text{Fe}(\text{3-bpp})_2][\text{MnCr}(\text{ox})_3]_2 \cdot (\text{3-bpp}) \cdot \text{MeOH}$, was highly disordered in the cations, allowing only the location of the central Fe(II) ions and six N atoms of the first coordination sphere. While they were successful in the observation of ferromagnetic ordering in the anion below 3 K, there was no conclusive evidence of a spin transition of the cations, which were found to be in a 1:1 HS:LS population. A later attempt to create hybrid materials based on $[\text{Fe}(\text{3-bpp})_2]^{2+}$ cations used $[\text{Cu}(\text{pds})_2]^-$ (pds = pyrazine-2,3-diselenoate) as the counter-ion,¹²⁶ but was also hindered by the absence of spin crossover in the cation, which remained in the HS configuration on varying the temperature.

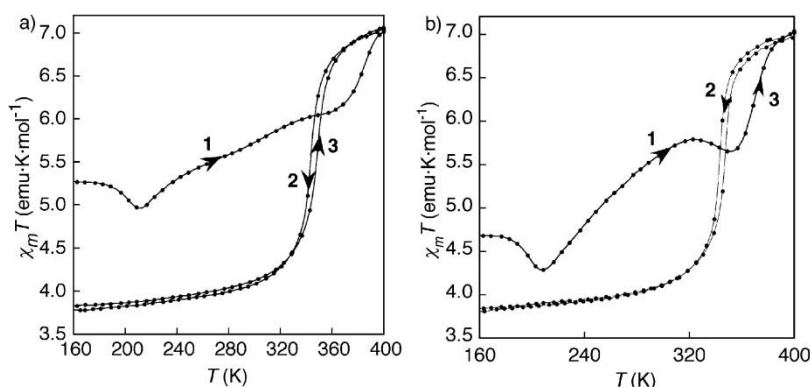


Figure 1.19: (left) Temperature dependence of χT for the compound $[\text{Fe}(\text{3-bpp})_2][\text{Cr}(\text{phen})(\text{ox})_2]_2 \cdot 0.5\text{H}_2\text{O} \cdot 0.5\text{MeOH}$. (right) The measurement repeated after re-hydration of the sample. Taken from reference 130.

In another series of publications,¹²⁷⁻¹²⁹ the same group tested the reversible absorption/desorption of water molecules in compounds containing various metal oxalates as the anion accompanying the $[\text{Fe}(\text{3-bpp})_2]^{2+}$ cation, and found that it could lead to the modulation of SCO behaviour.¹³⁰ When freshly synthesised, the compound $[\text{Fe}(\text{3-bpp})_2][\text{Cr}(\text{phen})(\text{ox})_2]_2 \cdot 0.5\text{H}_2\text{O} \cdot 0.5\text{MeOH}$ (phen = 1,10-phenanthroline) is associated with the variable temperature magnetic properties labelled **1** in Figure 1.19 (a). At the lowest temperatures measured, the molar magnetic susceptibility is consistent with the presence of 50% of the Fe(II) ions in the HS state, which the authors were also able to confirm via single crystal X-ray diffraction studies. Heating (**1**) the compound induces a dehydration process that yields the anhydrous form of the system, $[\text{Fe}(\text{3-bpp})_2][\text{Cr}(\text{phen})(\text{ox})_2]_2$. Performing a cooling and heating run on this form of the compound reveals an abrupt spin transition associated with a hysteresis loop. (**2** and **3** in Figure 1.19 (a)). The system was then rehydrated, and found to give the magnetic properties in Figure 1.19 (b). The value of χT found at low temperature contradicts the obtained structural data, in that it is indicative of a HS population of 28%, while the crystal structure contained the cation fully in the LS state. This rehydrated form of the compound could also be dehydrated, leading to the previously observed SCO behaviour.

An usual structural topology was found by Gass *et al.*, when they attempted to combine the potential host-guest chemistry of *N,N'*-bis(4-pyridyl-methyl)diaza-18-crown-6 (bpmdc) with $[\text{Fe}(\text{3-bpp})_2]^{2+}$ cations.¹³¹ By reacting the perchlorate salt of Fe(II) with 3-bpp, KNCS_e, and bpmdc in a mixture of ethanol, methanol and dichloromethane they were able to obtain the compound $[\text{Fe}(\text{3-bpp})_2][\text{bpmdcK}](\text{SeCN})_{1.7}(\text{ClO}_4)_{1.3} \cdot \text{MeOH} \cdot \text{H}_2\text{O}$. The diaza-crown coordinates the K^+ ions in the equatorial positions of the metal, and the axial positions are occupied by perchlorate anions. Each perchlorate then links to an adjacent bpmdcK moiety, extending in one dimension to form a chain (Figure 1.20). The 4-pyridyl-methyl branches of the ring then reach out, with the terminal nitrogen atom forming a hydrogen bond to the pyrazolyl group of the $[\text{Fe}(\text{3-bpp})_2]^{2+}$ cations. At room temperature, this compound is mostly in the LS state, with a small residual HS fraction. Heating to 400 K brings about the loss of the solvent molecules in the lattice, and the anhydrous form of the compound shows a gradual spin crossover centred at $T_{1/2} = 303$ K in the cooling mode.

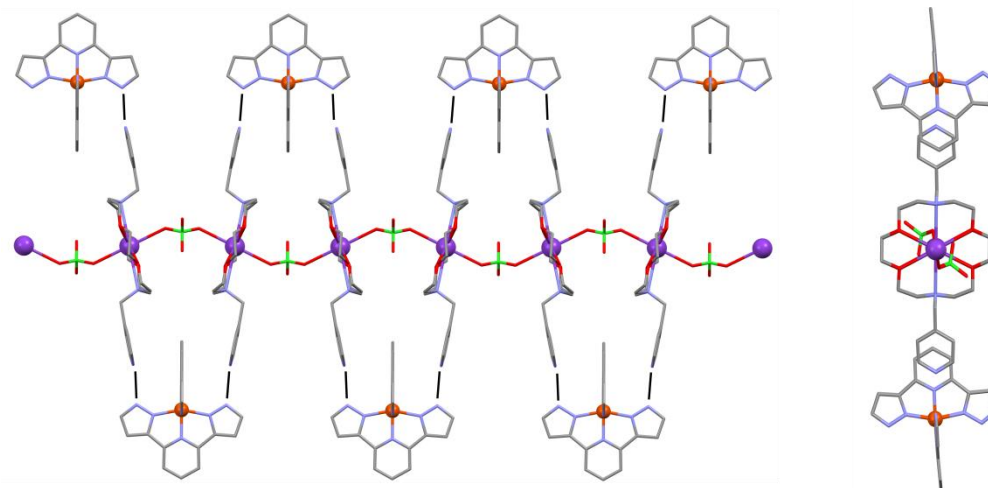


Figure 1.20: Crystal packing in the compound

$[\text{Fe}(3\text{-bpp})_2][\text{bpmcK}](\text{SeCN})_{1.7}(\text{ClO}_4)_{1.3}\cdot\text{MeOH}\cdot\text{H}_2\text{O}$. Hydrogen atoms are omitted for clarity, and the black lines represent hydrogen bonding between the pyrazolyl rings and the arms of the functionalised crown molecule. Adapted from reference 131.

While all of the above systems involve 3-bpp in the context of an Fe(II) cation where two molecules bind through their three central nitrogen atoms to the transition metal centre, there is one example of a dinuclear Fe(II) complex in the literature containing 3-bpp: $[(\text{Fe}(3\text{-bpp})(\text{NCS})_2)_2(4,4'\text{-bipy})]\cdot 2\text{CH}_3\text{OH}$, (4,4'-bipy = 4,4'-bipyridine) (Figure 1.21).¹³² This combination of metal centres within a single molecule leads to several possibilities in terms of the SCO behaviour. If the transition is complete, there may be a single switch of both metal centres, or it may be that they pass through an intermediate HS-LS phase before reaching the fully LS state. In this compound the transition was only partial, with half of the Fe(II) ions remaining in the quintet state. As a result there are two different possible scenarios for the switch, which have been denoted as Cases A and B.¹³³ In Case A systems, there is a spin transition of only one of the metal centres in *all* of the molecules. Case B corresponds to the *full* transition of only *half* of the molecules. A detailed crystallographic study was undertaken by Kaiba and co-workers to delineate these potential distributions of the HS ions.¹³⁴ The authors were able to identify three phases associated with compound. Phase I is observed above 161 K and, consistent with the magnetic behaviour, contains two equivalent Fe(II) centres in the HS state. On lowering the temperature, there is a phase transition, leading to Phase II, in which the HS Fe(II) ions are no longer crystallographically equivalent. By decreasing the temperature further, the partial spin crossover was induced to generate Phase III, and the switch observed to belong to Case A. Shepherd *et al.* further developed the work on this system

by demonstrating crystallographically and via Raman spectroscopy that the spin switch could be induced through the application of pressure.²²

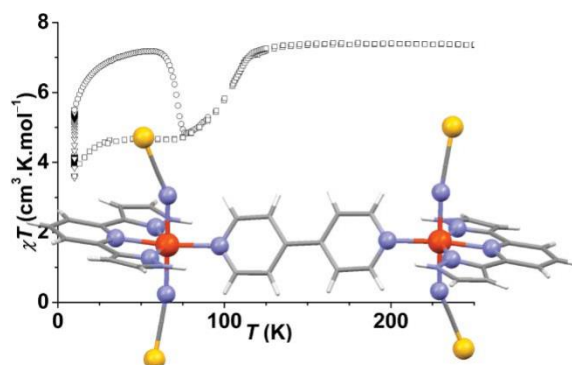


Figure 1.21: Magnetic properties of the compound $[(\text{Fe}(3\text{-bpp})(\text{NCS})_2)_2(4,4'\text{-bipy})]\cdot 2\text{CH}_3\text{OH}$, with the molecular structure superimposed. Figure taken from reference 134.

1.6 Aim and scope of the thesis

Despite the apparent richness of SCO behaviour described above for 3-bpp systems, at the time of undertaking this thesis there were no published examples of the use of synthetic derivatives of 3-bpp in this field of research.* This was remarked upon by Olguín and Brooker, who attributed this lack of 3-bpp analogues not to a lack of interest, but to “synthetic issues”.¹³⁵ Therefore, the initial challenge set out was to develop a methodology that would allow the synthesis of functionalised 3-bpp ligands. Once obtained, these ligands would then be used for the generation of mononuclear Fe(II) compounds, with a view to study their macroscopic properties. Provided that this strategy was successful, and depending on the availability of structural data, an attempt would then be made to outline correlations between the observed magnetic properties and the relationship between the lattice entities, both spin-active and –inactive. The development of this work is detailed over the course of the following Chapters.

Chapter 2 contains the synthetic procedures and experimental details for the physical characterisation of the compounds obtained. Chapter 3 then describes the development of the novel polypyrazolyl ligands that have been designed for the subsequent investigation of their coordination chemistry. The magneto-structural properties of a new $[\text{Fe}(3\text{-bpp})_2]^{2+}$ salt are described, and the compound shown to display a gradual spin crossover.

* The system based on 3-mbpp = 2,6-bis(5-methylpyrazol-3-yl)pyridine was published subsequent to the start of this thesis.

Chapters 4 and 5 provide an in-depth study of a mononuclear compound, $[\text{Fe}(\text{H}_4\text{L})_2](\text{ClO}_4)_2 \cdot \text{H}_2\text{O} \cdot 2(\text{CH}_3)_2\text{CO}$ (**1**), containing one of the polypyrazolyl ligands. A strongly cooperative spin transition is found to be intimately related to the structure and level of disorder within the lattice. This conclusion is supported by a description of the thermally trapped crystal structure. The photo-physical properties of **1** are then described, through the study of its meta-stable HS phase, which is distinct to the thermally trapped meta-stable HS phase. A Raman spectroscopy study of the system is then used to observe photo-switching within the hysteresis loop, and as a means of following the pressure-induced spin switch.

Chapters 6 and 7 use compound **1** as the basis of an investigation into the effect of varying the anions and solvents within the lattice on the magnetic properties and crystal packing. A case where the spin crossover becomes more cooperative on ageing the compound is described. Chapter 8 details the compounds obtained using another 3-bpp derivative, which results in the formation of distorted structures that do not display SCO.

In Chapter 9, the structural data provided by this thesis is collated with that found in the CSD for mononuclear Fe(II) systems with 3-bpp ligands. The data is then analysed from two points of view: a first, which involves previously defined parameters for the distortion of the cations, both in terms of their shape and in terms of the coordination sphere using Continuous Symmetry Measures.¹³⁶⁻¹³⁸ And a second, which uses Hirshfeld surface analysis to look at the bonding motifs and intermolecular interactions that are observed in the novel compounds obtained in this thesis. Chapter 10 offers conclusions based on the results obtained in this thesis.

1.7 References

1. N. Robertson and G. T. Yee, in *Molecular Materials*, John Wiley & Sons, Ltd, 2010, pp. 143-209.
2. J. Ribas, *Coordination Chemistry*, Wiley VCH., 2008.
3. P. Gütllich, A. Hauser and H. Spiering, *Angew. Chem. Int. Ed.*, 1994, **33**, 2024-2054.
4. K. Pandurangan, B. Gildea, C. Murray, C. J. Harding, H. Mueller-Bunz and G. G. Morgan, *Chem.-Eur J.*, 2012, **18**, 2021-2029.
5. P. N. Martinho, B. Gildea, M. M. Harris, T. Lemma, A. D. Naik, H. Mueller-Bunz, T. E. Keyes, Y. Garcia and G. G. Morgan, *Angew. Chem.- Int. Ed.*, 2012, **51**, 12597-12601.
6. G. G. Morgan, K. D. Murnaghan, H. Muller-Bunz, V. McKee and C. J. Harding, *Angew. Chem.- Int. Ed.*, 2006, **45**, 7192-7195.
7. D. Sertphon, D. J. Harding, P. Harding, K. S. Murray, B. Moubaraki, J. D. Cashion and H. Adams, *Eur. J. Inorg. Chem.*, 2013, 788-795.
8. C. Krüger, P. Augustín, I. Nemeč, Z. Trávníček, H. Oshio, R. Boča and F. Renz, *Eur. J. Inorg. Chem.*, 2013, 902-915.
9. I. Nemeč, R. Herchel, R. Boca, Z. Travnicek, I. Svoboda, H. Fuess and W. Linert, *Dalton Trans.*, 2011, **202**, 2020.
10. M. Griffin, S. Shakespeare, H. J. Shepherd, C. J. Harding, J.-F. Letard, C. Desplanches, A. E. Goeta, J. A. K. Howard, A. K. Powell, V. Mereacre, Y. Garcia, A. D. Naik, H. Mueller-Bunz and G. G. Morgan, *Angew. Chem.- Int. Ed.*, 2011, **50**, 896-900.
11. P. N. Martinho, C. J. Harding, H. Mueller-Bunz, M. Albrecht and G. G. Morgan, *Eur. J. Inorg. Chem.*, 2010, 675-679.
12. J. Tang, J. S. Costa, S. Smulders, G. Molnar, A. Bousseksou, S. J. Teat, Y. Li, G. A. van Albada, P. Gamez and J. Reedijk, *Inorg. Chem.*, 2009, **48**, 2128-2135.
13. S. Hayami, M. R. Karim and Y. H. Lee, *Eur. J. Inorg. Chem.*, 2013, **2013**, 683-696.
14. K. Bhar, S. Khan, J. S. Costa, J. Ribas, O. Roubeau, P. Mitra and B. K. Ghosh, *Angew. Chem.- Int. Ed.*, 2012, **51**, 2142-2145.
15. S. Hayami, Y. Komatsu, T. Shimizu, H. Kamihata and Y. H. Lee, *Coord. Chem. Rev.*, 2011, **255**, 1981-1990.
16. P. Gütllich, Y. Garcia and H. A. Goodwin, *Chem. Soc. Rev.*, 2000, **29**, 419-427.
17. A. Hauser, *Top. Curr. Chem.*, 2004, **233**, 49-58.
18. J. F. Létard, S. Asthana, H. J. Shepherd, P. Guionneau, A. E. Goeta, N. Suemura, R. Ishikawa and S. Kaizaki, *Chem.-Eur. J.*, 2012, **18**, 5924-5934.
19. C. H. Shih, C. F. Sheu, K. Kato, K. Sugimoto, J. Kim, Y. Wang and M. Takata, *Dalton Trans.*, 2010, **39**, 9794-9800.
20. C. Carbonera, J. S. Costa, V. A. Money, J. Elhaik, J. A. K. Howard, M. A. Halcrow and J. F. Létard, *Dalton Trans.*, 2006, 3058-3066.
21. H. W. Liu, A. Fujishima and O. Sato, *Appl. Phys. Lett.*, 2005, **86**, 122511.
22. H. J. Shepherd, P. Rosa, L. Vendier, N. Casati, J.-F. Letard, A. Bousseksou, P. Guionneau and G. Molnar, *Phys. Chem. Chem. Phys.*, 2012, **14**, 5265-5271.
23. H. J. Shepherd, T. Palamarciuc, P. Rosa, P. Guionneau, G. Molnar, J.-F. Letard and A. Bousseksou, *Angew. Chem.-Int. Ed.*, 2012, **51**, 3910-3914.
24. H. J. Shepherd, S. Bonnet, P. Guionneau, S. Bedoui, G. Garbarino, W. Nicolazzi, A. Bousseksou and G. Molnár, *Phys. Rev. B*, 2011, **84**, 144107.

25. A. Bousseksou, F. Varret, M. Goiran, K. Boukheddaden and J. P. Tuchagues, *Top. Curr. Chem.*, 2004, **235**, 65-84.
26. X. Bao, H. J. Shepherd, L. Salmon, G. Molnar, M.-L. Tong and A. Bousseksou, *Angew. Chem.- Int. Ed.*, 2013, **52**, 1198-1202.
27. C. Bartual-Murgui, L. Salmon, A. Akou, N. A. Ortega-Villar, H. J. Shepherd, M. Carmen Munoz, G. Molnar, J. Antonio Real and A. Bousseksou, *Chem.-Eur J.*, 2012, **18**, 507-516.
28. R.-J. Wei, J. Tao, R.-B. Huang and L.-S. Zheng, *Inorg. Chem.*, 2011, **50**, 8553-8564.
29. G. J. Halder, C. J. Kepert, B. Moubaraki, K. S. Murray and J. D. Cashion, *Science*, 2002, **298**, 1762.
30. P. Gütllich and H. A. Goodwin, *Top. Curr. Chem.*, 2004, **233**, 1-47.
31. C. M. Klug, A. M. McDaniel, S. R. Fiedler, K. A. Schulte, B. S. Newell and M. P. Shores, *Dalton Trans.*, 2012, **41**, 12577-12585.
32. S. A. Barrett, C. A. Kilner and M. A. Halcrow, *Dalton Trans.*, 2011, 12021-12024.
33. Z. Ni, A. M. McDaniel and M. P. Shores, *Chem. Sci.*, 2010, **1**, 615-621.
34. Z. Ni and M. P. Shores, *J. Am. Chem. Soc.*, 2008, **131**, 32-33.
35. P. Gamez, J. S. Costa, M. Quesada and G. Aromí, *Dalton Trans.*, 2009, 7845-7853.
36. H. Spiering, *Top. Curr. Chem.*, 2004, **235**, 171-195.
37. H. Spiering and N. Willenbacher, *J. Phys.-Condes. Matter*, 1989, **1**, 10089-10105.
38. N. Willenbacher and H. Spiering, *J. Phys. C*, 1988, **21**, 1423-1439.
39. P. Gütllich, A. B. Gaspar and Y. Garcia, *Beilstein J. Org. Chem.*, 2013, **9**, 342-391.
40. A. F. Orchard, *Magnetochemistry*, Oxford University Press, 2003.
41. J. H. Van Vleck, *The Theory of Electric and Magnetic Susceptibilities*, Oxford University Press, 1932.
42. J. Tao, R.-J. Wei, R.-B. Huang and L.-S. Zheng, *Chem. Soc. Rev.*, 2012, **41**, 703-737.
43. M. A. Halcrow, *Chem. Soc. Rev.*, 2011, **40**, 4119-4142.
44. S. K. Wolff, D. J. Grimwood, J. J. McKinnon, M. J. Turner, D. Jayatilaka and M. A. Spackman, 2012, University of Western Australia.
45. M. A. Spackman and D. Jayatilaka, *CrystEngComm*, 2009, **11**, 19-32.
46. J. J. McKinnon, M. A. Spackman and A. S. Mitchell, *Acta Cryst. B*, 2004, **60**, 627-668.
47. M. A. Spackman and J. J. McKinnon, *CrystEngComm*, 2002, 378-392.
48. P. Guionneau, M. Marchivie, G. Bravic, J.-F. Létard and D. Chasseau, *Top. Curr. Chem.*, 2004, **234**, 97-128.
49. V. A. Money, I. R. Evans, M. A. Halcrow, A. E. Goeta and J. A. K. Howard, *Chem. Commun.*, 2003, 158-159.
50. J. M. Holland, J. A. McAllister, C. A. Kilner, M. Thornton-Pett, A. J. Bridgeman and M. A. Halcrow, *J. Chem. Soc. Dalton Trans.*, 2002, 548-554.
51. M. Marchivie, P. Guionneau, J. F. Letard and D. Chasseau, *Acta Cryst. B*, 2003, **59**, 479-486.
52. J. K. McCusker, A. L. Rheingold and D. N. Hendrickson, *Inorg. Chem.*, 1996, **35**, 2100-2112.
53. M. G. B. Drew, C. J. Harding, V. McKee, G. G. Morgan and J. Nelson, *J. Chem. Soc., Chem. Commun.*, 1995, 1035-1038.

54. M. Lorenc, C. Balde, W. Kaszub, A. Tissot, N. Moisan, M. Servol, M. Buron-Le Cointe, H. Cailleau, P. Chasle, P. Czarnecki, M. L. Boillot and E. Collet, *Phys. Rev. B*, 2012, **85**.
55. E. Collet, N. Moisan, C. Balde, R. Bertoni, E. Trzop, C. Laulhe, M. Lorenc, M. Servol, H. Cailleau, A. Tissot, M.-L. Boillot, T. Graber, R. Henning, P. Coppens and M. Buron-Le Cointe, *Phys. Chem. Chem. Phys.*, 2012, **14**, 6192-6199.
56. E. Collet, M. Lorenc, M. Cammarata, L. Guerin, M. Servol, A. Tissot, M.-L. Boillot, H. Cailleau and M. Buron-Le Cointe, *Chem.-Eur. J.*, 2012, **18**, 2051-2055.
57. A. Tissot, R. Bertoni, E. Collet, L. Toupet and M.-L. Boillot, *J. Mater. Chem.*, 2011, **21**, 18347-18353.
58. M. Sorai and S. Seki, *J. Phys. Soc. Jpn.*, 1972, **33**, 575.
59. E. Konig and K. Madeja, *Inorg. Chem.*, 1967, **6**, 48.
60. M. Sorai, *Top. Curr. Chem.*, 2004, **235**, 153-170.
61. J. P. Tuchagues, A. Bousseksou, G. Molnar, J. J. McGarvey and F. Varret, *Top. Curr. Chem.*, 2004, **235**, 85-103.
62. J. A. Wolny, R. Diller and V. Schünemann, *Eur. J. Inorg. Chem.*, 2012, 2635-2648.
63. W. R. Browne and J. J. McGarvey, *Coord. Chem. Rev.*, 2006, **250**, 1696-1709.
64. S. Bedoui, G. Molnar, S. Bonnet, C. Quintero, H. J. Shepherd, W. Nicolazzi, L. Salmon and A. Bousseksou, *Chem. Phys. Lett.*, 2010, **499**, 94-99.
65. S. Bonhommeau, G. Molnár, A. Galet, A. Zwick, J. A. Real, J. J. McGarvey and A. Bousseksou, *Angew. Chem.-Int. Ed.*, 2005, **44**, 4069-4073.
66. S. Cobo, D. Ostrovskii, S. Bonhommeau, L. Vendier, G. Molnar, L. Salmon, K. Tanaka and A. Bousseksou, *J. Am. Chem. Soc.*, 2008, **130**, 9019-9024.
67. O. Kahn, *Molecular Magnetism*, Wiley VCH, 1993.
68. C. P. Slichter and H. Drickamer, *J. Chem. Phys.*, 1972, **56**, 2142.
69. M. Sorai and S. Seki, *J. Phys. Chem. Sol.*, 1974, **35**, 555-570.
70. J. Pavlik and R. Boča, *Eur. J. Inorg. Chem.*, 2013, 697-709.
71. H. Paulsen, V. Schünemann and J. A. Wolny, *Eur. J. Inorg. Chem.*, 2013, 628-641.
72. J. J. McGarvey and I. Lawthers, *J. Chem. Soc.-Chem. Commun.*, 1982, 906-907.
73. S. Decurtins, P. Gütllich, K. M. Hasselbach, A. Hauser and H. Spiering, *Inorg. Chem.*, 1985, **24**, 2174-2178.
74. S. Decurtins, P. Gütllich, C. P. Kohler, H. Spiering and A. Hauser, *Chem. Phys. Lett.*, 1984, **105**, 1-4.
75. A. Hauser, *J. Chem. Phys.*, 1991, **94**, 2741-2748.
76. A. Hauser, *Chem. Phys. Lett.*, 1986, **124**, 543-548.
77. A. Hauser, *Top. Curr. Chem.*, 2004, **234**, 155-198.
78. M. Marchivie, P. Guionneau, J. F. Létard, D. Chasseau and J. A. K. Howard, *J. Phys. Chem. Solids*, 2004, **65**, 17-23.
79. M. A. Halcrow, *Chem. Soc. Rev.*, 2008, **37**, 278-289.
80. A. Hauser, *Chem. Phys. Lett.*, 1992, **192**, 65-70.
81. J.-F. Létard, P. Guionneau, L. Rabardel, J. A. K. Howard, A. E. Goeta, D. Chasseau and O. Kahn, *Inorg. Chem.*, 1998, **37**, 4432-4441.
82. J. F. Létard, *J. Mater. Chem.*, 2006, **16**, 2550-2559.
83. J. F. Létard, P. Guionneau, O. Nguyen, J. S. Costa, S. Marcen, G. Chastanet, M. Marchivie and L. Goux-Capes, *Chem.-Eur. J.*, 2005, **11**, 4582-4589.
84. A. Hauser, A. Vef and P. Adler, *J. Chem. Phys.*, 1991, **95**, 8710-8717.
85. A. Hauser, *Coord. Chem. Rev.*, 1991, **111**, 275-290.

86. Various, *Eur. J. Inorg. Chem.*, 2013, 574-1067.
87. O. Roubeau, *Chem.-Eur J.*, 2012, **18**, 15230-15244.
88. M. A. Halcrow (ed.), *Spin-Crossover Materials: Properties and Applications*, Wiley-VCH, 2013.
89. P. Guionneau, F. Le Gac, A. Kaiba, J. S. Costa, D. Chasseau and J.-F. Letard, *Chem. Commun.*, 2007, 3723-3725.
90. J. S. Costa, P. Guionneau and J. F. Letard, *J. Phys. Conf. Ser.*, 2005, **21**, 67-72.
91. M. Nihei, H. Tahira, N. Takahashi, Y. Otake, Y. Yamamura, K. Saito and H. Oshio, *J. Am. Chem. Soc.*, 2010, **132**, 3553-3560.
92. N. F. Sciortino, K. R. Scherl-Gruenwald, G. Chastanet, G. J. Halder, K. W. Chapman, J.-F. Letard and C. J. Kepert, *Angew. Chem.- Int. Ed.*, 2012, **51**, 10154-10158.
93. S. Bonnet, M. A. Siegler, J. S. Costa, G. Molnár, A. Bousseksou, A. L. Spek, P. Gamez and J. Reedijk, *Chem. Commun.*, 2008, 5619-5621.
94. S. Bonnet, G. Molnár, J. S. Costa, M. A. Siegler, A. L. Spek, A. Bousseksou, W. T. Fu, P. Gamez and J. Reedijk, *Chem. Mat.*, 2009, **21**, 1123-1136.
95. S. Pillet, E. Bendeif, S. Bonnet, H. J. Shepherd and P. Guionneau, *Phys. Rev. B*, 2012, **86**, 064106.
96. S. Bedoui, M. Lopes, S. Zheng, S. Bonnet, G. Molnar and A. Bousseksou, *Adv. Mat.*, 2012, **24**, 2475-2478.
97. S. Bedoui, M. Lopes, W. Nicolazzi, S. Bonnet, S. Zheng, G. Molnar and A. Bousseksou, *Phys. Rev. Lett.*, 2012, **109**.
98. O. Kahn, J. Krober and C. Jay, *Adv. Mat.*, 1992, **4**, 718-728.
99. O. Kahn and C. J. Martinez, *Science*, 1998, **279**, 44-48.
100. J. F. Létard, P. Guionneau and L. Goux-Capes, *Top. Curr. Chem.*, 2004, **235**, 221-249.
101. E. Coronado, J. R. Galán-Mascarós, M. Monrabal-Capilla, J. Garcia-Martinez and P. Pardo-Ibañez, *Adv. Mat.*, 2007, **19**, 1359-1360.
102. J. R. Galán-Mascarós, E. Coronado, A. Forment-Aliaga, M. Monrabal-Capilla, E. Pinilla-Cienfuegos and M. Ceolin, *Inorg. Chem.*, 2010, **49**, 5706-5714.
103. F. Prins, M. Monrabal-Capilla, E. A. Osorio, E. Coronado and H. S. J. van der Zant, *Adv. Mat.*, 2011, **23**, 1545-1549.
104. V. Meded, A. Bagrets, K. Fink, R. Chandrasekar, M. Ruben, F. Evers, A. Bernard-Mantel, J. S. Seldenthuis, A. Beukman and H. S. J. van der Zant, *Phys. Rev. B*, 2011, **83**, 245415.
105. G. Felix, K. Abdul-Kader, T. Mahfoud, I. y. A. Gural'skiy, W. Nicolazzi, L. Salmon, G. Molnar and A. Bousseksou, *J. Am. Chem. Soc.*, 2011, **133**, 15342-15345.
106. H. Tran Quang, F. Terki, S. Kamara, M. Dehbaoui, S. Charar, B. Sinha, C. Kim, P. Gandit, I. y. A. Gural'skiy, G. Molnar, L. Salmon, H. J. Shepherd and A. Bousseksou, *Angew. Chem.- Int. Ed.*, 2013, **52**, 1185-1188.
107. S. Titos-Padilla, J. M. Herrera, X. W. Chen, J. J. Delgado and E. Colacio, *Angew. Chem.- Int. Ed.*, 2011, **50**, 3290-3293.
108. L. Salmon, G. Molnar, D. Zitouni, C. Quintero, C. Bergaud, J.-C. Micheau and A. Bousseksou, *J. Mater. Chem.*, 2010, **20**, 5499-5503.
109. C. M. Quintero, I. y. A. Gural'skiy, L. Salmon, G. Molnar, C. Bergaud and A. Bousseksou, *J. Mater. Chem.*, 2012, **22**, 3745-3751.
110. Y. Lin and S. A. Lang, *J. Heterocycl. Chem.*, 1977, **14**, 435.
111. H. A. Goodwin and K. H. Sugiyarto, *Chem. Phys. Lett.*, 1987, **139**, 470-474.
112. K. H. Sugiyarto and H. A. Goodwin, *Aust. J. Chem.*, 1988, **41**, 1645-1663.

113. M. L. Scudder, D. C. Craig and H. A. Goodwin, *CrystEngComm*, 2005, **7**, 642-649.
114. K. H. Sugiyarto, D. C. Craig, A. D. Rae and H. A. Goodwin, *Aust. J. Chem.*, 1994, **47**, 869-890.
115. T. Buchen, P. Gütllich, K. H. Sugiyarto and H. A. Goodwin, *Chem.-Eur J.*, 1996, **2**, 1134-1138.
116. S. Marcén, L. Lecren, L. Capes, H. A. Goodwin and J.-F. Létard, *Chem. Phys. Lett.*, 2002, **358**, 87-95.
117. A. Bhattacharjee, V. Ksenofontov, K. H. Sugiyarto, H. A. Goodwin and P. Gütllich, *Adv. Funct. Mat.*, 2003, **13**, 877-882.
118. R. Pritchard, C. A. Kilner and M. A. Halcrow, *Chem. Commun.*, 2007, 577-579.
119. J. McMurtrie and I. Dance, *CrystEngComm*, 2005, **7**, 216-229.
120. M. A. Halcrow, *Coord. Chem. Rev.*, 2005, **249**, 2880-2908.
121. K. H. Sugiyarto, M. L. Scudder, D. C. Craig and H. A. Goodwin, *Aust. J. Chem.*, 2000, **53**, 755-765.
122. M. L. Scudder, H. A. Goodwin and I. G. Dance, *New J. Chem.*, 1999, **23**, 695-705.
123. T. D. Roberts, F. Tuna, T. L. Malkin, C. A. Kilner and M. A. Halcrow, *Chem. Sci.*, 2012, **3**, 349-354.
124. C. M. Grunert, H. A. Goodwin, C. Carbonera, J.-F. Létard, J. Kusz and P. Gütllich, *J. Phys. Chem. B*, 2007, **111**, 6738-6747.
125. E. Coronado, J. R. Galán Mascarós, M. C. Giménez-López, M. Almeida and J. C. Waerenborgh, *Polyhedron*, 2007, **26**, 1838-1844.
126. E. Coronado, J. C. Dias, M. C. Giménez-López, C. Giménez-Saiz and C. J. Gómez-García, *J. Mol. Struct.*, 2008, **890**, 215-220.
127. M. Clemente-León, E. Coronado, M. Carmen Giménez-López, F. M. Romero, S. Asthana, C. Desplanches and J.-F. Létard, *Dalton Trans.*, 2009, 8087-8095.
128. M. C. Giménez-López, M. Clemente-León, E. Coronado, F. M. Romero, S. Shova and J.-P. Tuchagues, *Eur. J. Inorg. Chem.*, 2005, 2783-2787.
129. E. Coronado, M. C. Giménez-López, C. Giménez-Saiz, J. M. Martínez-Agudo and F. M. Romero, *Polyhedron*, 2003, **22**, 2375-2380.
130. M. Clemente-León, E. Coronado, M. C. Giménez-López and F. M. Romero, *Inorg. Chem.*, 2007, **46**, 11266-11276.
131. I. A. Gass, S. R. Batten, C. M. Forsyth, B. Moubaraki, C. J. Schneider and K. S. Murray, *Coord. Chem. Rev.*, 2011, **255**, 2058-2067.
132. D. Fedouai, Y. Bouhadja, A. Kaiba, P. Guionneau, J. F. Letard and P. Rosa, *Eur. J. Inorg. Chem.*, 2008, 1022-1026.
133. A. B. Gaspar, M. C. Muñoz and J. A. Real, *J. Mater. Chem.*, 2006, **16**, 2522-2533.
134. A. Kaiba, H. J. Shepherd, D. Fedouai, P. Rosa, A. E. Goeta, N. Rebbani, J. F. Letard and P. Guionneau, *Dalton Trans.*, 2010, **39**, 2910-2918.
135. J. Olguín and S. Brooker, *Coord. Chem. Rev.*, 2011, **255**, 203-240.
136. S. Alvarez, *J. Am. Chem. Soc.*, 2003, **125**, 6795-6802.
137. S. Alvarez, D. Avnir, M. Llunell and M. Pinsky, *New J. Chem.*, 2002, **26**, 996-1009.
138. H. Zabrodsky, S. Peleg and D. Avnir, *J. Am. Chem. Soc.*, 1992, **114**, 7843-7851.

